3330–3350 *Nucleic Acids Research, 2016, Vol. 44, No. 7* *Published online 04 February 2016*
doi: 10.1093/nar/gkw061

Kissing-loop interaction between 5′ and 3′ ends of tick-borne Langat virus genome 'bridges the gap' between mosquito- and tick-borne flaviviruses in mechanisms of viral RNA cyclization: applications for virus attenuation and vaccine development

Konstantin A. Tsetsarkin[1], Guangping Liu[1], Kui Shen[2] and Alexander G. Pletnev[1,*]

[1]Laboratory of Infectious Diseases, National Institute of Allergy and Infectious Diseases (NIAID), National Institutes of Health (NIH), Bethesda, MD, 20892-3203 USA and [2]Bioinformatics and Computational Biosciences Branch, NIAID, NIH, Bethesda, MD, 20892, USA

Received September 10, 2015; Revised January 20, 2016; Accepted January 24, 2016

ABSTRACT

Insertion of microRNA target sequences into the flavivirus genome results in selective tissue-specific attenuation and host-range restriction of live attenuated vaccine viruses. However, previous strategies for miRNA-targeting did not incorporate a mechanism to prevent target elimination under miRNA-mediated selective pressure, restricting their use in vaccine development. To overcome this limitation, we developed a new approach for miRNA-targeting of tick-borne flavivirus (Langat virus, LGTV) in the duplicated capsid gene region (DCGR). Genetic stability of viruses with DCGR was ensured by the presence of multiple *cis*-acting elements within the N-terminal capsid coding region, including the stem-loop structure (5′SL6) at the 3′ end of the promoter. We found that the 5′SL6 functions as a structural scaffold for the conserved hexanucleotide motif at its tip and engages in a complementary interaction with the region present in the 3′ NCR to enhance viral RNA replication. The resulting kissing-loop interaction, common in tick-borne flaviviruses, supports a single pair of cyclization elements (CYC) and functions as a homolog of the second pair of CYC that is present in the majority of mosquito-borne flaviviruses. Placing miRNA targets into the DCGR results in superior attenuation of LGTV in the CNS and does not interfere with development of protective immunity in immunized mice.

INTRODUCTION

Tick-borne flaviviruses form a monophyletic group of tick-transmitted pathogens within the *Flavivirus* genus of the *Flaviviridae* family. Infection of birds and mammals, including humans, is associated with a variety of clinical symptoms that range from self-limited flu-like infections to severe forms of encephalitis or hemorrhagic fevers (1). Tick-borne encephalitis virus (TBEV) is the most important member of the group that causes more than 10 000 human cases annually in vast geographic ranges that include forested areas of Europe, Russia, China and Japan. Due to the lack of efficient antivirals against TBEV, public vaccination is considered the most effective strategy for controlling disease outbreaks (2). Currently available inactivated vaccines require multiple doses to establish primary immunity and repeated booster inoculations to maintain a protective response. As such the development of a live attenuated vaccine capable of eliciting lasting TBEV immunity following a single dose is warranted.

Initially isolated in 1950s from ticks in Malaysia, Langat virus (LGTV) was shown to be a naturally attenuated tick-borne flavivirus that did not cause human disease in the endemic area (3). It causes significantly less neurovirulence and neuroinvasiveness compared to TBEV when tested in mice and nonhuman primates (4,5). In the 1970s, several attenuated variants of LGTV were evaluated as live vaccine candidates in human volunteers in the US and Russia (5,6). Even though the studies were discontinued due to a relatively high incidence (1:18 000) of encephalitis among vaccinees, they showed that vaccination with LGTV provided durable protective immunity against TBEV (6). However, additional attenuation of LGTV-based vaccine candidates would be required to increase their safety.

*To whom correspondence should be addressed. Tel: +1 301 402 7754; Fax: +1 301 480 0501; Email: apletnev@niaid.nih.gov

We previously demonstrated that introduction of target sequences for cellular microRNAs (miRNA) into the genome of flaviviruses results in selective decreases in viral neurovirulence and/or host range restriction (7,8). Although escape mutants lacking intact miRNA target sequence can occur as a result of error prone flavivirus replication, simultaneous targeting of distant regions of virus genome generally results in increased stability of targeted viruses (9). Characterization of novel strategies for stable expression of multiple miRNA target sequences in flavivirus genomes is essential for development of safe live vaccine candidates utilizing the miRNA-based attenuation approach. Previously, it was demonstrated that separation of promoter/regulatory and protein/structural functions of the capsid protein (C) gene using a sequence duplication strategy allowed for stable expression of heterologous sequences in the background of several mosquito-borne flaviviruses (10–12). Here, we sought to investigate if a comparable approach could be applied to achieve the stable expression of functional miRNA target sequences in a background of LGTV.

Characterization of promoter elements located in the C gene region is critical for construction of viruses expressing heterologous sequences in the region of capsid gene duplication. Although the *cis*-acting elements of the C gene of mosquito-borne flaviviruses have been extensively studied [(13–15) and reviewed in (16)], relatively little is known about the role of these elements within the C gene of tick-borne flaviviruses (17–19), and no promoter elements within the gene of LGTV have been described so far.

MATERIALS AND METHODS

Plasmids

To simplify the process of virus recovery, the infectious cDNA clone p689 of wild-type TP-21 strain of LGTV (GenBank access #AF253419) (20) has been modified by substituting the pBR322 cloning vector and SP6 promoter with the low-copy number pACNR1811 cloning vector and eukaryotic RNA Pol II promoter from cytomegalovirus (CMV) using a strategy described previously (8,21). Hepatitis delta virus ribozyme and RNA Pol II terminator sequences were cloned after the 3′ end of the LGTV genome to ensure release of the authentic 3′-end of nascent RNA during transcription. Two intron sequences were introduced at nt positions 2495 and 9180 of TP-21 genome to reduce plasmid toxicity during propagation in *Escherichia coli* (strain MC1061). The resulting plasmid (designated wt) was used as a genetic background for construction of all CMV-based clones. All functional sequences used for construction were amplified from plasmid DNAs published previously (8) using Phusion DNA polymerase (New England Biolabs [NEB], Ipswich, MA, USA) and assembled individually or in combination using conventional cloning methods (22). Sequences encoding the 2A protease from foot and mouth disease virus (FMDV), the codon-optimized LGTV capsid protein gene (131–408 nt), and the duplicated LGTV E/NS1 (2171–2488 nt) gene region were assembled using a polymerase chain reaction (PCR)-based technique (22). Target sequences for all brain- or tick-specific miRNAs, as well as their mutated versions, are summarized in Supplementary Table S1.

To generate sub-genomic LGTV replicons capable of nano-Luciferase (nLuc) gene expression, the cDNA genome of C58 virus was modified by deletion of sequence (731–748 nt) encoding six amino acids (AA) that constitute a cleavage site for furin protease in the prM protein. An nLuc gene was amplified from pNL1.1 (Promega, Madison, WI, USA) and was fused with the codon-optimized sequence of an E/NS1 stem-anchor region (2171–2488 nt). This cassette was introduced in-frame at nt position 2489 of the LGTV genome, to generate the polyprotein topology that was described earlier (9,23).

Since the LGTV cDNA genome that does not contain intron sequences and cannot be propagated in the pACNR1811 vector due to its toxicity for *E. coli*, the cDNA replicon was generated on the platform of the p689 cDNA clone under transcriptional control of an SP6 promoter. The resulting plasmid was designated RepC58 and was used as template to introduce mutations into the 5′ and/or 3′ end of genome, and to generate a 'non-replicating' LGTV replicon that lacks sequence between 2768 and 8770 nt and encodes 2001 AA of non-structural proteins. Genetic integrity of each plasmid was verified by restriction enzyme digestions and sequence analysis. Sequence and detailed information for all plasmid constructs are available from the authors upon request.

Cells and viruses

Vero (African green monkey kidney) cells were cultured in Opti-Pro medium (Invitrogen) supplemented with 2% fetal bovine serum (FBS), 2 mM L-glutamine and 50 μg/ml of gentamicin. The virus titer in each preparation was determined on Vero cells using an immunostaining plaque-forming assay as described previously (24). Briefly, each virus sample was 10-fold serially diluted in duplicate with Opti-Pro medium and used to infect Vero cells in 24-well plates for 1 h at 37°C. One milliliter of Opti-MEM containing 1% methylcellulose (Invitrogen), 2% FBS, 2 mM L-glutamine and 50 μg/ml of gentamicin was added to each well, and plates were incubated at 37°C and 5% CO_2 for 5 days. Cells were fixed for 20 min with 100% methanol, and plaques were visualized by immunostaining with TBEV-specific hyperimmune mouse ascitic fluid and peroxidase-labeled anti-mouse IgG (Dako Co, Carpinteria, CA, USA).

DNA transfection and virus recovery

Infectious viruses were rescued from plasmid DNA using the method described previously (8). Briefly, 5 μg of plasmid DNA were transfected into 1.2×10^6 Vero cells seeded onto a 12.5-cm^2 flask using Lipofectamine 2000 reagent (Invitrogen). Cells were washed twice with Opti-MEM and maintained at 37°C and 5% CO_2 for 5 days in 5 ml of Dulbecco's modified Eagle's medium supplemented with 10% FBS and 1× Penicillin-Streptomycin-Glutamine (PSG) solution. Aliquots of cell culture medium (0.5 ml) were collected daily and stored at −80°C followed by virus titration in Vero cells.

Immunofluorescence

On the fifth day post DNA transfection, Vero cells in 12.5-cm^2 flasks were washed twice with phosphate buffered saline (PBS) and fixed in 100% methanol for 15 min. Cells were treated for 1 h with primary TBEV antibodies diluted 1:1000 with Opti-Pro medium supplemented with 2% FBS. LGTV antigens were detected by staining with TBEV-specific antibodies in the hyperimmune mouse ascitic fluid and fluorescein-labeled goat anti-mouse IgG (KPL) at a 1:1000 dilution, followed by image visualization using a Leica DMI 4000B fluorescent microscope.

Replicon study

To generate 5′-capped RNA transcripts from each replicon construct, plasmid DNA (5 μg) was linearized with EcoRV restriction endonuclease (NEB, Ipswich, MA, USA), followed by *in vitro* transcription from the SP6 promoter using the mMESSAGE mMACHINE kit (Ambion, Austin, TX, USA) according to manufacturer's instructions. Equal amounts (5 μg) of each RNA were electroporated into 5 × 10^7 Vero cells using a Gene Pulser Xcell electroporation system (Bio-Rad, Hercules, CA, USA) as described previously (8). Cells were diluted in 50 ml of L-15 medium supplemented with 10% FBS/1× PSG solution, and 1 ml of cells were plated into each well of a 24-well plate. The cells were allowed to recover for 2 h at 37°C, followed by a media change to 1 ml of Opti-Pro supplemented with 2% FBS and 2 mM L-glutamine. The cells were incubated at 37°C and 5% CO_2 until nLuc measurements were taken according to the manufacturer's instructions (Promega, Madison, WI, USA). Briefly, medium from three wells of the 24-well plate was removed. Cells were washed once with PBS and lysed in 0.3 ml of 1× Pierce Luciferase Cell Lysis Buffer (Thermo Scientific) for 10 min at 37°C with constant shaking. Lysates were diluted 1, 10, 100 or 1000-fold with PBS (depending on a preliminary reading) and 50 μl sample aliquots were mixed with 50 μl of 2× nanoGlo substrate (Promega), followed by measurements of nLuc activity using a Synergy HT microplate reader (BioTech, Winooski, VT, USA). Results are given as a normalized average value of two reads for cell extracts from three independent wells.

To demonstrate that replicons are not capable of secondary cell infection, aliquots of cell-culture supernatants from electroporated Vero cells were collected every 24 h post RNA transfection up to 7 dpi and titrated in Vero cells using the plaque-forming assay. Infectious virus foci were not detected for any of the engineered replicon constructs.

Serial passaging and genetic stability of miRNA targeted viruses in Vero cells

For the first passage, Vero cells in 25-cm^2 flasks were infected at an MOI of 0.01 with viruses harvested at 5 days post DNA transfection and incubated at 37°C and 5% CO_2 for 3 days (for viruses with a titer of 10^7 pfu/ml or higher in Vero cells supernatant by 5 dpi) or for 5 days (for viruses with a titer below 10^7 pfu/ml). At the end of the first passage viruses in cell-culture medium were diluted 1/10 with Opti-Pro medium, and 1 ml of inoculum was used to infect 25-cm^2 flasks of fresh Vero cells. The process was repeated 10 times. At the end of the tenth passage, viral RNA was extracted from 0.14 ml of supernatant using the QIAamp Viral RNA Mini kit (Qiagen) and regions of interest were amplified using the Titan One Tube RT-PCR kit (Roche, Indianapolis, IN, USA) and sequenced.

Ethics statement

All animal experiments were performed in compliance with the guidelines of the NIAID/NIH Institutional Animal Care and Use Committee. The NIAID DIR Animal Care and Use Program acknowledges and accepts responsibility for the care and use of animals involved in activities covered by the NIH IRP's PHS Assurance #A4149-01, last issued on 6 November 2011.

Evaluation of viruses in mice

Viruses were diluted to 4 $\log_{10}$(pfu/ml) with L-15 medium supplemented with 1× SPG (218 mM sucrose, 6 mM L-glutamic acid, 3.8 mM KH_2PO_4, 7.2 mM K_2HPO_4, pH 7.2), and 3-day-old Swiss Webster mice (Taconic, Hudson, NY, USA) in groups of 10 were inoculated intracranially (IC) with 10 μl (100 pfu) of virus. The brains from three mice were harvested on days 3, 5 and 7 post-infection (dpi), and virus titer in each brain homogenate was determined in Vero cells as described previously (8). Differences in replication kinetics were compared using 2-way ANOVA, followed by *P*-value adjustment using Tukey's method implemented in Prism 6 software (La Jolla, CA, USA). To validate the ANOVA model, residuals, which are the observed values minus the grand mean, the effect of different viruses, and the effect of different time points, were calculated using statistical software R (25). The Quantile–Quantile Plot and scatter plot of residuals are shown in Supplementary Figure S1 and indicate that residuals have an independent and identical distribution.

To assess the effect of miRNA targeting in the duplicated C gene region or in the 3′ NCR on virus neurovirulence, 3-day-old Swiss Webster mice were inoculated IC with 1, 10 or 100 pfu of miRNA targeted viruses and monitored for morbidity and mortality for 21 dpi. Mice that developed clinical signs of encephalitis were humanely euthanized. Brains from moribund (paralyzed) animals were harvested, and viral RNA from brain homogenates was extracted and used for sequence analysis of virus genome. Differences in mouse survival were compared using log-rank (Mantel-Cox) test implemented in Prism 6 software.

To evaluate the immunogenicity of miRNA-targeted viruses, groups of five 3-week-old female C3H mice (Taconic) were infected intraperitoneally with 10^5 pfu of C48–124(2)/9/1-E5 virus or mock inoculated with L-15 medium supplemented with 1× SPG and monitored for signs of neurotropic disease daily until 28 dpi. Mice were bled on 1 dpi for detection of virus in serum and on 28 dpi for measurement of neutralizing antibody titer using the plaque reduction neutralization assay ($PRNT_{50}$) against LGTV TP-21 strain as described previously (26). On 29 dpi, mice were challenged intraperitoneally with 10^4 pfu of LGTV TP-21 strain, and blood was collected on the next day to evaluate viremia. Mice were monitored for morbidity for an additional 28 days.

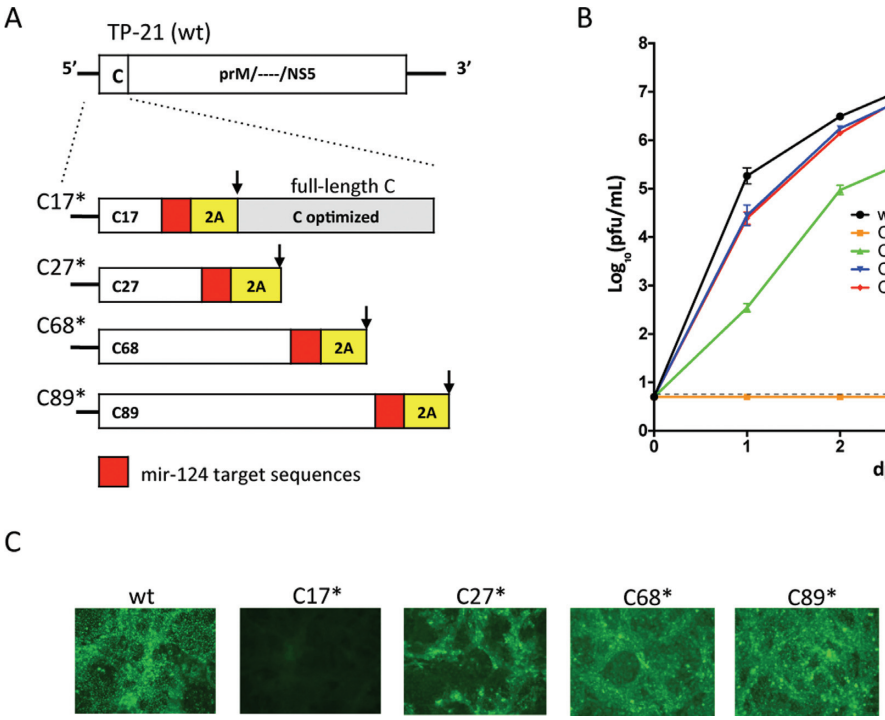

Figure 1. Growth of LGTV with DCGR in Vero cells. (**A**) Schematic representation of viral genomes used in this study. Target sequence for mir-124 is indicated as red box, and sequence of 2A protease from FMDV is highlighted as yellow box. Cleavage site for 2A protease is indicated by black arrow. Gray areas represent codon optimized C protein gene sequence. C17 AA, C27 AA, C68 AA and C89 AA boxes represent the duplicated regions of 5′ end of C protein gene encoding 17, 27, 68 and 89 AA of truncated C protein, respectively. (**B**) Growth kinetics of infectious virus recovered after plasmid DNA transfection into Vero cells. Individual samples for each time point from one biological replica were titrated in Vero cells in duplicate, and results are presented as an average ± standard deviation (shown as error bars). The dashed line indicates the limit of virus detection [0.7 $\log_{10}$(pfu/ml)]. (**C**) Immunofluorescence analysis. Representative images show the expression of LGTV antigens in Vero cells on day 5 post-transfection with indicated pDNA construct.

Modeling of secondary structure of viral RNAs

RNA secondary structures were predicted using m-fold web server for nucleic acid folding using default parameters (27). To visualize regions that are likely to be involved in flavivirus genome cyclization, hybrid sequence consisting of 330 nt of 5′ and 330 nt of 3′ genome ends was generated. The resulting sequence of 660 nt was subjected to folding analysis using the same parameters for folding as authentic viral sequences. The following sequences for representative strains of tick- and mosquito-borne flaviviruses were selected for the folding analysis: LGTV strain TP-21 (GenBank access #AF253419), TBEV strain Neudoerfl (# U27495), Omsk hemorrhagic fever virus strain Bogoluvovska (#AY193805), Powassan virus strain LB (#L06436), dengue type 4 virus strain 814669 (# AY648301), yellow fever virus strain Asibi (# AY640589.1), West Nile virus strain NY99-flamingo382–99 (#AF196835.2) and Zika virus strain MR766 (#NC012532).

RESULTS

Development of Langat viruses with duplicated capsid gene regions (DCGR)

To map the sequence within the C gene involved in LGTV replication, a set of infectious clones was generated featuring gradual lengthening of the 5′-terminus of the C gene followed by target sequence for neuron-specific mir-124 miRNA. To ensure a release of a functional C protein, the sequence for the 2A protease from FMDV was inserted upstream of a second copy of a codon-optimized full-length sequence of the C gene (C-opt) and was followed by the rest of LGTV TP-21 genome (Figure 1A). The resulting constructs were designated as C17*, C27*, C68* and C89*, reflecting the portion of the authentic C gene retained in the virus. Transfection of the plasmids into Vero cells demonstrated that preservation of the C27 AA (but not C17 AA) region resulted in recovery of infectious virus; however, replication of C27* virus was attenuated by ∼50-fold compared to C68* virus. Enlargement of the truncated C region from 68 to 89 AA had no effect on growth kinetics of recovered LGTV (Figure 1B and C), suggesting that the C68 AA region contains all appropriate *cis*-acting elements necessary and sufficient for efficient LGTV growth.

Nucleotide sequence conveys functionality of the C68 AA region. To establish if nucleotide or amino acid sequence conveys functionality of the C68 AA region in LGTV replication, two additional clones (C68 FrSh1 and C68 FrSh2) were generated that contained open reading frame (ORF) shifts due to insertion of a single adenine residue after AA codon C8 or C19, respectively. To restore the ORF for downstream gene translation, the deletion of a guanine residue at nt position 334 was also incorporated into these clones. These modifications were designed to exert a min-

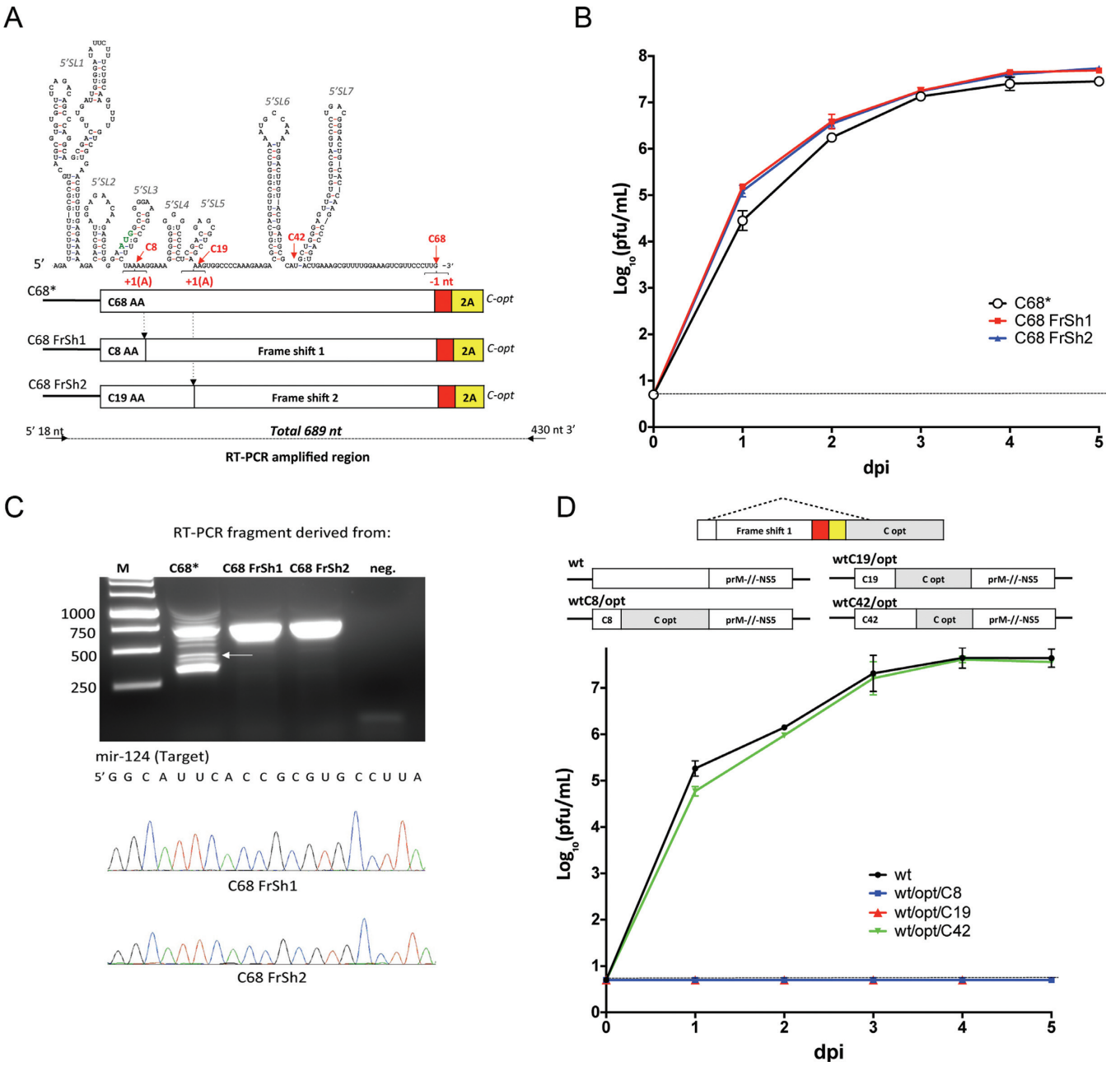

Figure 2. Growth and genetic stability in Vero cells of LGTV with ORF shifting mutations. (**A**) Top: stem-loop structure for the 5′ end of LGTV TP-21 genome. Middle: schematic representation of viral genomes used in the study. Positions of ORF-shifting insertion (+1 nt) of a single A nucleotide (C8 and C19) and position of reading frame restoration (−1 nt at C68 position) are indicated. Bottom: diagram indicating relative position of primers used for RT-PCR analysis of LGTV genomes. (**B**) Growth kinetics of infectious virus recovered after plasmid DNA transfection into Vero cells. Aliquots of cell culture samples harvested at indicated time from one biological replica were titrated in Vero cells in duplicate. Results are presented as an average ± standard deviation. (**C**) Top: results of RT-PCR analysis of indicated virus genomes isolated after ten passages in Vero cells. White arrow indicates the position of DNA fragment produced by RT-PCR and corresponding to the size of DNA fragment derived from unmodified parental LGTV genome. Bottom: results of sequence analysis of mir-124 target region for C68 FrSh1 and C68 FrSh2 virus amplicons that are shown above. (**D**) Top: schematic representation of hypothetical reversion of C68 FrSh1 and C68 FrSh2 genomes to wt-like LGTV containing chimeric C protein gene sequence. Viral genomes (wtC8/opt, wtC19/opt and wtC42/opt) containing 8, 19 or 42 AA codons of wt LGTV C protein gene and the rest of codon-optimized C protein gene are shown. A wt sequence is indicated in white, and a codon-optimized sequence is in grey. Bottom: growth kinetics of recovered LGTV with chimeric capsid gene sequences in Vero cells. The dashed line indicates the limit of virus detection [0.7 $\log_{10}$(pfu/ml)].

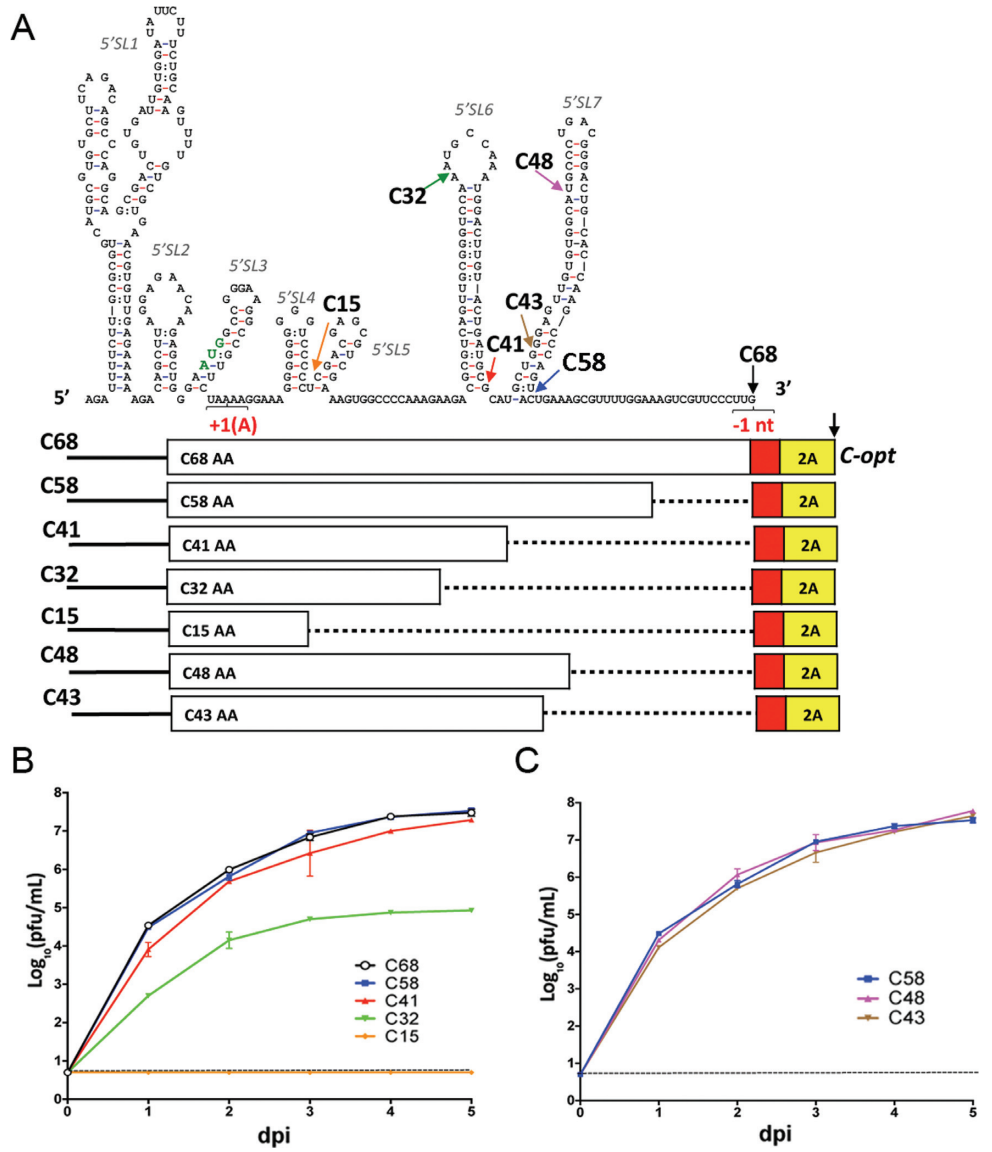

Figure 3. Mapping of a minimal region of C gene that is required for efficient LGTV growth in Vero cells. (**A**) Top: stem-loop structure of the 5′-end of TP-21 genome. Colored arrows indicate positions of fusion sites between wt C gene sequences and target sequence for mir-124 (red box). Bottom: schematic representation of viral genomes carrying the indicated portion of truncated C gene. (**B** and **C**) Growth kinetics of recovered viruses in Vero cells.

imal effect on RNA secondary structure, while disrupting an authentic AA sequence in the C68 truncated C protein (Figure 2A). Both C68 FrSh1 and C68 FrSh2 replicated slightly more efficiently in Vero cells than the unmodified C68* virus, indicating that only the nucleotide sequence of C68 and not the protein product is responsible for LGTV replication (Figure 2B). It is possible that a truncated capsid protein of C68* virus interferes with the full-length copy of the C protein (C-opt) during C68* virion assembly or negatively affects RNA translation or replication, resulting in the observed attenuation of virus growth.

ORF shifting mutations increase genetic stability of DCGR. ORF shifting mutations in the C68 AA region are thought to increase genetic stability of heterogeneous sequences inserted into the DCGR by preventing homologous recombination between two C gene sequences (wt C68 AA and C-opt). To test this, we subjected C68*, C68 FrSh1 and C68 FrSh2 viruses to 10 sequential passages in Vero cells, followed by RT-PCR analysis of viral RNA. As expected, C68* accumulated RNA genomes of various sizes, including a fragment corresponding to a complete deletion of the inserted sequences (Figure 2C highlighted with an arrow). In contrast, no point mutations or deletions were detected in C68 FrSh1 or C68 FrSh2 genomes including the target sequence for mir-124 miRNA as verified by sequence analysis (Figure 2C).

Sequence downstream of position C8 AA is critical for LGTV viability. Even though frame shifting increases stability of C68 FrSh1 and C68 FrSh2 viruses in the absence of miRNA-mediated selective pressure [Vero cells do not express mir-124 (7)], the question remains whether formation of viable wild-type-like genomes is theoretically possi-

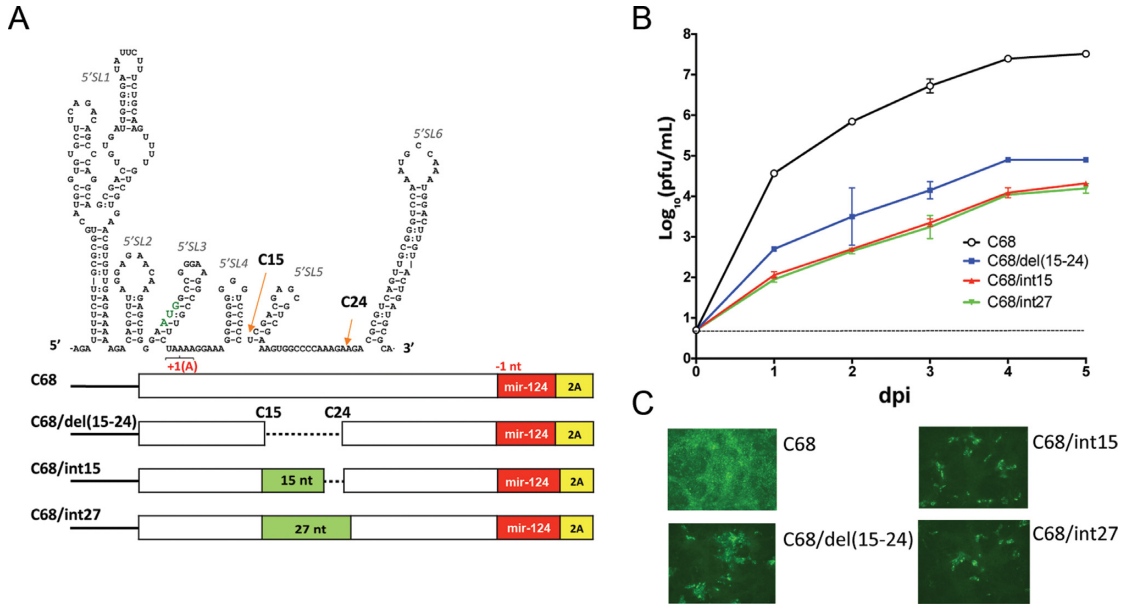

Figure 4. Role of sequence between C15 AA and C24 AA of C gene on growth of LGTV in Vero cells. (**A**) Top: stem-loop structure of the 5′-end of TP-21 genome. Orange arrows indicate the end of C15 AA and C24 AA regions in the C gene sequence. Target sequence for mir-124 is highlighted as red box. Bottom: schematic representation of C68 genomes and its derivatives used in the study. Green boxes indicate the position and nt length of inserted sequences. (**B**) Growth kinetics of recovered viruses in Vero cells. (**C**) Immunofluorescence analysis of LGTV antigen expression in Vero cells on day 5 post-transfection with indicated DNA constructs.

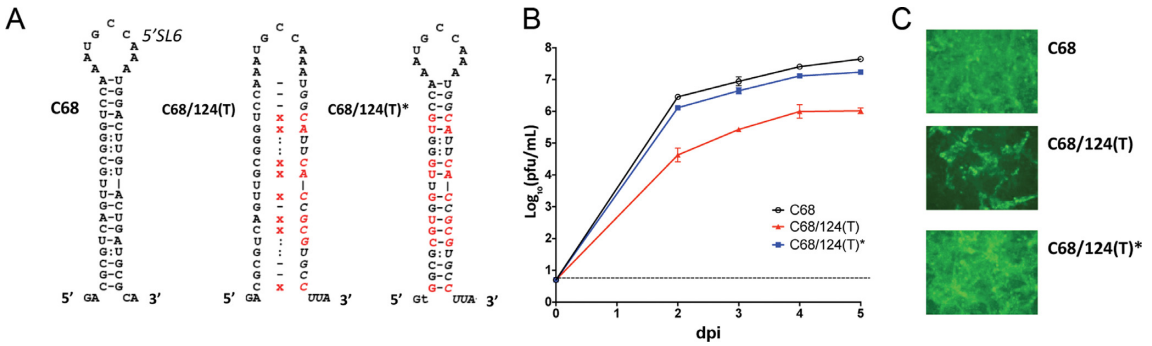

Figure 5. Significance of stem-loop organization of the 5′SL6 for virus growth in Vero cells. (**A**) The predicted secondary structure of 5′SL6 in C68 genome was destabilized by mutations (highlighted in red) in the 3′ strand to create the C68/124(T) virus. The 5′SL6-like secondary structure was restored in C68/124(T) by introducing a set of compensatory complementary mutations in the 5′ strand of 5′SL6 to create the C68/124(T)* virus. (**B**) Growth kinetics of rescued viruses in Vero cells. Aliquots of viruses in cell cultures were harvested at indicated time points from one biological replica, and virus titers were determined in Vero cells in duplicate. (**C**) Results of immunofluorescence assay for LGTV antigens in Vero cells on day 5 post-transfection are shown.

ble for the modified viruses as a result of homologous recombination between DCGR sequences. To address this, we engineered three LGTV clones with chimeric C protein containing different portions of wt and C-opt sequences (Figure 2D). The junction region was placed after AA codon 8, 19 and 42 of the wt C sequence in wtC8/opt, wtC19/opt and wtC42/opt, respectively. Position C42 AA was chosen arbitrarily to generate a positive control virus that contains sequences from about half of the wt C protein and half of C-opt. Neither wtC8/opt nor wtC19/opt constructs yielded infectious progeny in Vero cells, whereas growth kinetics of viruses recovered from wtC42/opt and wt clones of LGTV were similar (Figure 2D). These data indicate that *cis*-acting element(s) located downstream of positions C8 and C19 AA are critical for LGTV viability. Therefore, in order for ORF shifting viruses to revert to wild-type genome, two independent mutations have to be accrued simultaneously: (i) frameshift restoration and (ii) deletion of a DCGR. As a result, strategies involving separation of nucleotide/regulatory and protein/structural functions of the C gene in combination with ORF shifting mutations might have superior genetic stability in miRNA-targeted viruses compared to previously described approaches (7,9,28), which do not incorporate a mechanism for preventing formation of viable wild-type-like viral genomes under miRNA mediated selective pressure.

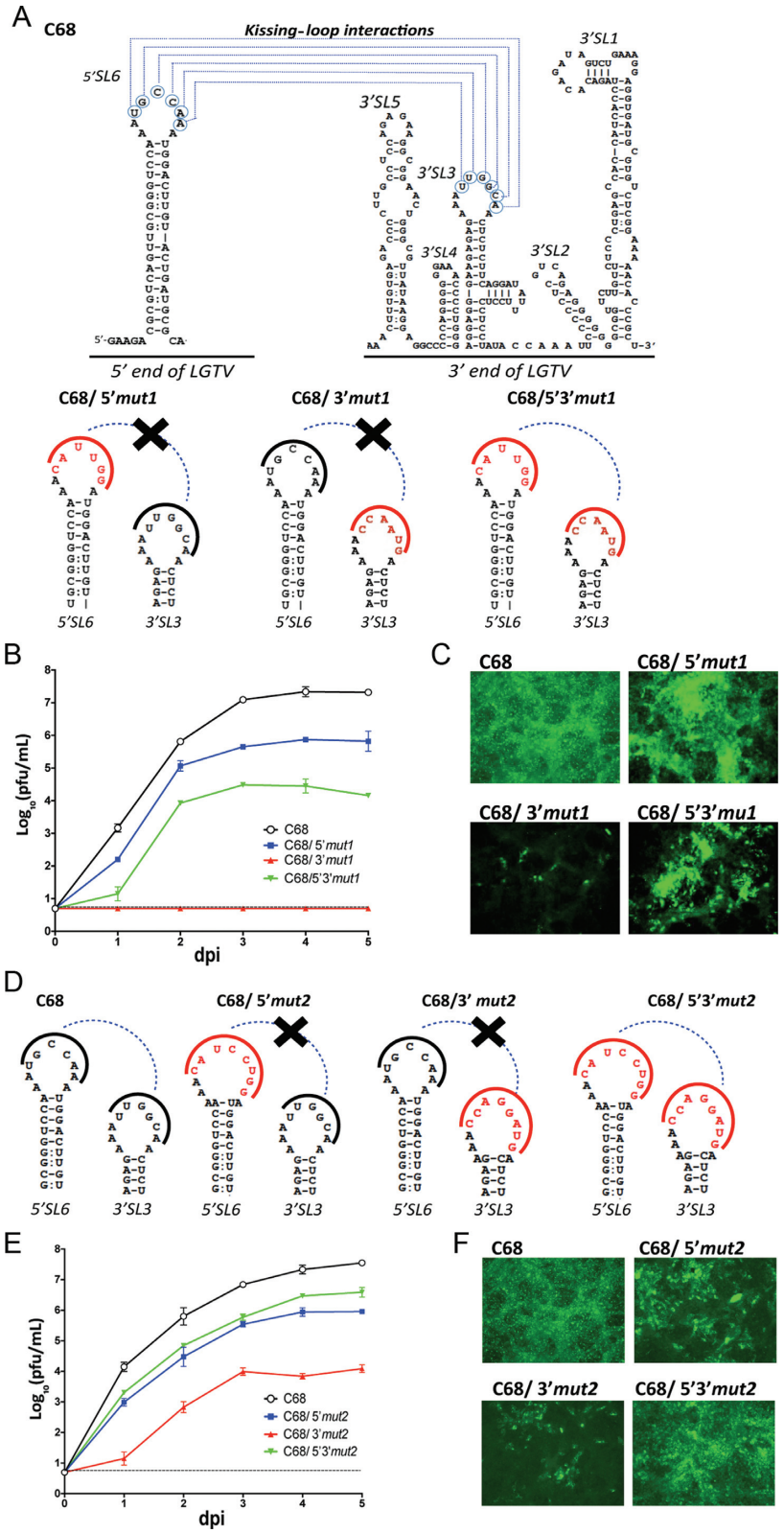

Figure 6. Kissing-loop interaction between 5′ and 3′ ends of LGTV genome. (**A**) Top: secondary structures and predicted interactions between the 5′SL6 and 3′SL3 (3′NCR) in the C68 genome. Nucleotide residues involved in complementary interactions are in blue circles connected by dashed lines. Bottom: hexanucleotide motifs at the tip of 5′SL6 and/or 3′SL3 C68 virus were substituted with 5′*mut*1 or 3′*mut*1 sequences (highlighted in red) to generate C68/5′*mut1*, C68/3′*mut1* or C68/5′3′*mut1* viruses. Potential kissing-loop contact is represented by blue dashed line, which can be destabilized by *mut*1 substitutions (crossed blue dashed line). (**B** and **E**) Growth kinetics of recovered viruses after DNA transfection into Vero cells. (**C** and **F**) Immunofluorescence analysis of LGTV antigen expression in Vero cells on day 5 post-transfection. (**D**) Schematic representation of mutations that disrupted or restored interaction between the sequences at the tips of 5′SL6 and 3′SL3 in the C68 genome. Introduced substitutions (5′*mut2* or 3′*mut2* sequences) are highlighted in red.

Characterization of the *cis*-acting elements within the capsid gene

Mapping of a minimal promoter region within the capsid gene. The separation of promoter/enhancer and protein/structural functions of the C gene region in C68 FrSh1 (hereafter C68 FrSh1 virus will be referred to as C68) facilitates detailed analysis of the 5′-end regulatory elements in the context of an infectious virus. Since the kinetics of wtC42/opt virus recovery were almost identical to the parental wt construct, we hypothesized that the 5′ promoter region might be significantly shorter than the C68 AA region (Figures 1 and 2D). To determine the size of the minimum C gene region required for efficient LGTV replication, a set of clones containing gradual deletion of the 3′ terminal sequence of the putative C gene promoter region was generated in Vero cells (Figure 3A). Growth kinetics of virus recovery for C48 was indistinguishable as compared to C58 and C68 clones, however, subsequent larger deletions of C gene resulted in LGTV attenuation of various degrees (Figure 3B and C). This demonstrates that the promoter activity is localized to the gene region encoding only the 48 N-terminal AA of C protein.

The role of C15-C24 AA region in LGTV replication. Secondary RNA structure of the C gene sequence of LGTV was predicted using m-fold analysis (Figure 4A) revealing almost identical to TBEV folding pattern. For TBEV the 5′ end secondary structure was validated experimentally supporting the existence of the 5′SL2, 5′SL3, 5′SL4 and 5′SL6 (19,29). Considering a substantial sequence homology between 5′ ends of LGTV and TBEV genomes (about 88% at the nucleotide level for the 5′SL2 - 5′SL6 region), we rationalized that similar folding structure is likely to be attained by 5′ end of LGTV. To understand the role of *cis*-acting elements within the C48 AA promoter region in the regulation of LGTV replication in Vero cells, we focused on the sequence downstream of position C15AA. This sequence is located downstream of the predicted stem-loop structures 3 and 4 (5′SL3 and 5′SL4; Figure 3A), which have been characterized previously in the context of TBEV replication in BHK-21 cells (29). First, we analyzed the role of sequences located in a region between AA C15 and C24. This region includes 5′SL5, which is not present in TBEV, and the prolonged inter-stem region (Figure 4A). The deletion of that region in C68/del(15–24) resulted in almost an 500-fold reduction of virus titer in Vero cells, indicating it is an important factor for LGTV replication (Figure 4B and C). Even though the deletion of 24 nt in C68/del(15–24) did not affect the predicted folding of the remaining stem-loop structures in the 5′ end of the LGTV genome (Supplementary Figure S2), it is possible that this deletion disrupts relative organization of *cis*-acting elements within the C48 AA promoter. To address this, we inserted two random sequences of 15 and 27 nt into the deleted region of C68/del(15–24). The latter (C68/int27) was designed to restore the length and secondary structure of the 5′ promoter region, including restoration of 5′SL5-like structure (Supplementary Figure S2). However, both constructs (C68/int15 and C68/int27) were even more attenuated for growth in Vero cells compared to C68/del(15–24) (Figure 4B and C), suggesting that the primary structure, but not overall secondary stem-loop organization, determines functionality of the C15-C24 AA replication enhancer in LGTV.

The role of 5′SL6 structure in LGTV replication. Next, we analyzed the role of the region between positions C24 and C48 AA in regulation of LGTV replication. The importance of this region was evident by the fact that the C32 deletion mutant attained 200-fold lower titers in Vero cells as compared to the C68 construct (Figure 3B). This region forms 5′SL6, which is conserved among tick-borne flaviviruses, and was shown previously to be important for TBEV growth *in vitro* (19). To establish whether the primary nt sequence that forms the stem of 5′SL6 or whether the overall stem-like organization influences the kinetics of LGTV replication, we modified C68 by substituting the sequence that forms a 3′-strand of the 5′SL6 with a mir-124 target sequence, which destabilized the 5′SL6 secondary structure (Figure 5A). Replication of resulting virus C68/124(T) was reduced by 20-fold in Vero cells as compared to C68 (Figure 5B). However, introduction of compensatory mutations into the 5′ strand of the 5′SL6 of C68/124T virus that restored nt pairing between 5′ and 3′ strands resulted in an increase in C68/124(T)* replication to the level attained by the unmodified C68 virus (Figure 5B and C). These findings support the importance of the stem structure but not the primary nt sequence of 5′SL6 for virus replication.

A kissing-loop interaction between 5′SL6 and 3′SL3 regulates LGTV growth in Vero cells. The 6-nt sequence located at the tip of 5′SL6 was shown to be invariable among all tick-borne flaviviruses (19). To determine if this sequence is involved in regulation of LGTV replication, the 6 nt at the tip were substituted by transition mutations (*mut1*) in C68 to generate C68/5′*mut1* virus (Figure 6A). This mutation resulted in ∼30-fold reduction in virus titer in Vero cells at 4 and 5 days post pDNA transfection (Figure 6B and C). It was suggested previously (30) that the 6 nt at the tip of 5′SL6 could potentially be involved in complementary interaction with a hexanucleotide sequence located at the tip of a predicted 'dumbbell-like' structure 3′SL3 at the 3′end of the LGTV genome. To determine if 5′SL6 and 3′SL3 are involved in a so-called kissing-loop interaction, we restored sequence complementarity between the loops by introducing 6 nt transitions (3′*mut1*) in the 3′SL3 of C68/5′*mut1* virus to generate C68/5′3′*mut1* (Figure 6A, on top). For control (C68/3′*mut1*), the same substitutions were introduced into the 3′SL3 of C68 (Figure 6A). No replication was detected for C68/3′*mut1* virus after pDNA transfection (Figure 6B and C). In contrast, C68/5′3′*mut1*, although attenuated relative to C68 or C58/5′*mut1* (Figure 6B and C), was viable and replicated in Vero cells, reaching a titer of 4.5 $\log_{10}$(pfu/ml) by 3 dpi. This indicates that restoration of sequence complementarity between 5′SL6 and 3′SL3 in the context of C68/5′3′*mut1* virus is sufficient to redeem replication of C68/3′*mut1* virus. To confirm that the restored replication of C68/5′3′*mut1* virus was due to the complementary interactions between 5′SL6 and 3′SL3 of the LGTV genome, we generated a C68/5′3′*mut*2 virus, in which complementarity in the kissing-loops was

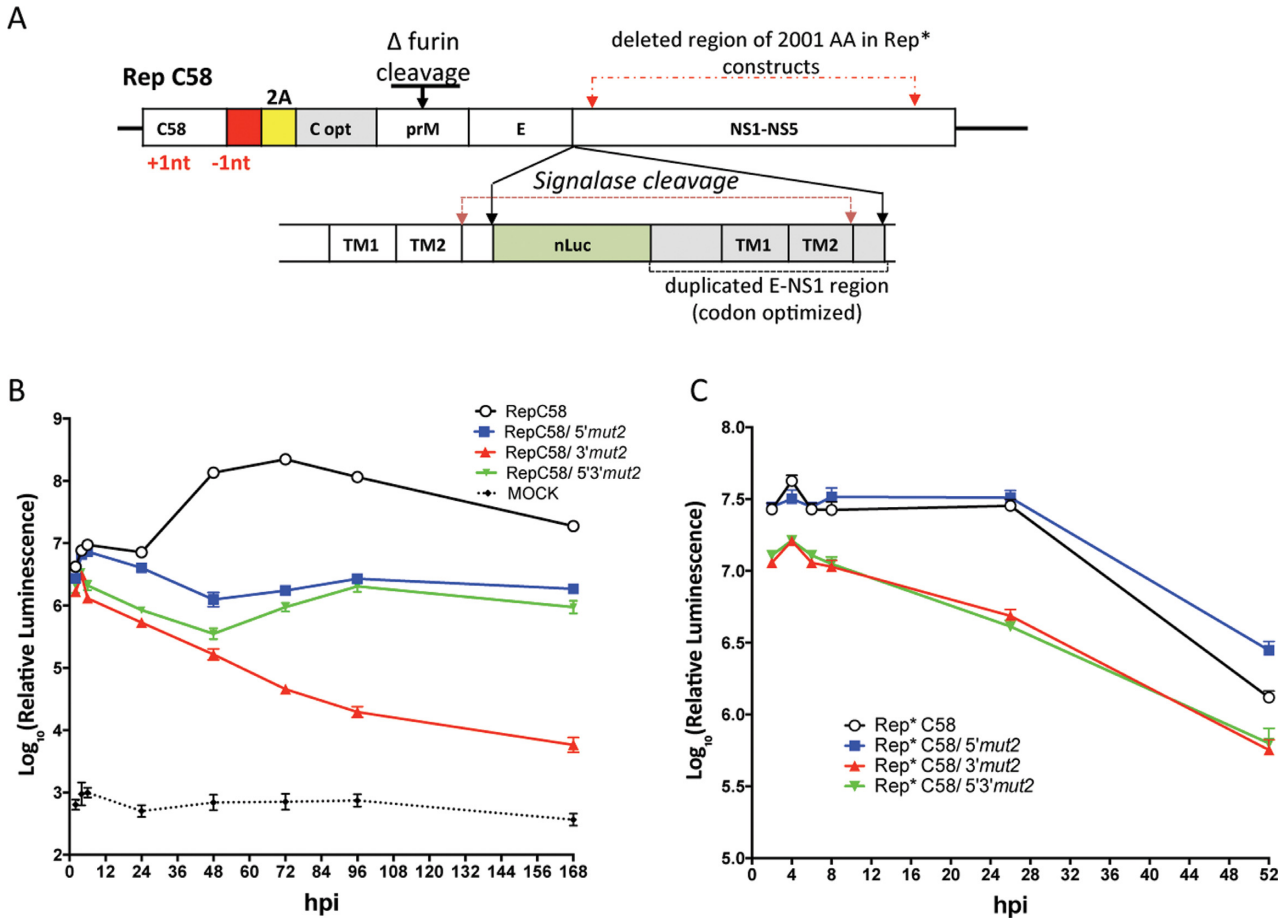

Figure 7. Kissing-loop interaction between 5′SL6 and 3′SL3 regulates LGTV replication but does not affect viral RNA translation. (**A**) Genetic organization of the RepC58 replicon that was constructed on the basis of C58 virus genome (Figure 3A). Regions of nLuc gene insertion and deletion of cleavage site for cellular furin protease are indicated. To generate RepC58/5′*mut2*, RepC58/3′*mut2* or RepC58/5′3′*mut2* replicons, hexanucleotide motifs at the tip of 5′SL6 and/or 3′SL3 of RepC58 replicon were substituted with 5′*mut2* and/or 3′*mut2* sequences (Figure 6A and D). Red arrows and dashed line indicate the region that was deleted to generate non-replicating replicons. Target sequence for mir-124 and 2A protease gene sequence from FMDV are indicated as red and yellow boxes, respectively. Positions of ORF shift insertion (+1 nt after a C8 AA codon) and frame shift restoration (−1 nt in a C58 codon) are shown. (**B**) Vero cells were mock-transfected or transfected with RNA transcripts of replication-competent replicons (a set of RepC58). (**C**) Vero cells were transfected with RNA transcripts of non-replicating versions of replicons (a set of Rep*C58). (**B** and **C**) Normalized kinetics of relative luminescence are presented as the mean values ± SD (shown as error bars) of two reads for 3 biological replicates of RNA-transfected Vero cell extracts.

expanded from 6 to 8 mutated nt (5′*mut2*) (Figure 6D). The C68/5′3′*mut2* virus, having complementary mutations in both kissing-loops, replicated more efficiently as compared to viruses C68/5′*mut2* and C68/3′*mut2,* which contained mutations only in separate loops located in the either 5′ or 3′ end of the LGTV genome (Figure 6E and F). Taken together, these results indicate that 5′SL6 likely functions as a scaffold for the hexanucleotide sequence located at its tip, enabling it to engage in a kissing-loop interaction with SL3 from the 3′ end of the LGTV genome.

Kissing-loop interaction controls the efficiency of LGTV genome replication. To differentiate which step of the LGTV life cycle is affected by the kissing-loop interaction, we developed a sub-genomic LGTV replicon capable of nLuc expression. For that, the infectious cDNA clone of C58 virus (C58 was chosen over C68 due to cloning convenience) was further modified by deletion of 6 AA codons encoding the cleavage site for furin cellular protease in the prM protein. This rendered the resulting virions completely non-infectious (31,32) and restricted cell-to-cell spreading of replicating LGTV genomes (Figure 7A). An nLuc gene was cloned in-frame within the duplicated E/NS1 region using topology described previously (9,23). The CMV-promoter-driven strategy for launching virus replication in cells was substituted with the conventional SP6 strategy for *in vitro* RNA transcription and delivery of viral RNAs into the cytoplasm of cells (see 'Materials and Methods' section). The resulting plasmid was designated RepC58 and was used as a template to incorporate 8 nt substitutions (*mut2*) into 5′SL6 and 3′SL3 (Figure 6D).

Electroporation of RNA transcripts produced from replicons into Vero cells showed that destabilization of the kissing-loop interaction by *mut2* substitutions in RepC58/5′*mut2* or RepC58/3′*mut2* resulted in a 100- or 10 000-fold reduction of nLuc gene activity, respectively (Figure 7B). However, restoration of kissing-loop complementarity in RepC58/5′3′*mut2* resulted in restoration of

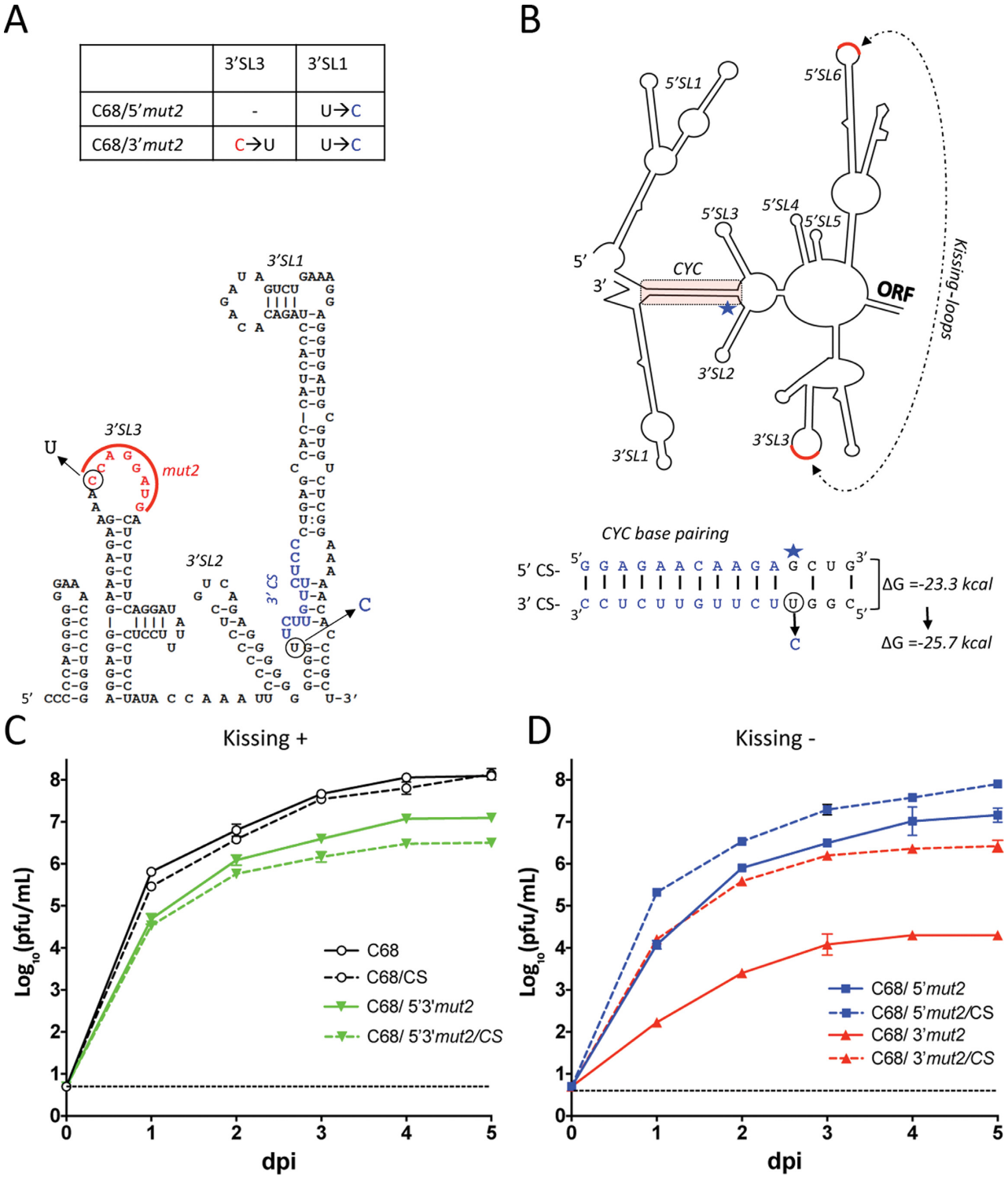

	3′SL3	3′SL1
C68/5′*mut2*	-	U→C
C68/3′*mut2*	C→U	U→C

Figure 8. Compensatory mutations in the 3′CYC element of LGTV compensate for dysfunctional kissing-loop contact. (**A**) Mutations that were identified in the genomes of C68/5′*mut2* and C68/3′*mut2* viruses after 10 passages in Vero cells. (**B**) Top: predicted RNA structure of 5′- and 3′-ends of LGTV genome. Cyclization element (CYC), a region of complementarity between 5′ cyclization sequence (CS) and 3′CS of CYC element, is highlighted in pink. Kissing-loop contact is shown as black dashed line. The blue star shows location of U→C substitution common for both Vero cell passaged viruses. Bottom: the same U→C substitution is shown in context of nt base pairing of 5′CS and 3′CS in the CYC element. Predicted ΔG values are given for the CYC structure with and without U→C substitution in the 3′CS. (**C** and **D**) Effect of U→C substitution (CS) on growth of viruses with unmodified (C68) and restored (C68/5′3′*mut2*) kissing-loop contacts (**C**) or viruses with impaired (C68/5′*mut2,* C68/3′*mut2*8) kissing-loop contacts (**D**) in Vero cells. Growth kinetics of engineered C68 and C68/5′3′*mut2* (**C**), or C68/5′*mut2* and C68/3′*mut2* (**D**) viruses with (shown as dashed lines) and without (shown as solid lines) U→C substitution in the 3′CS.

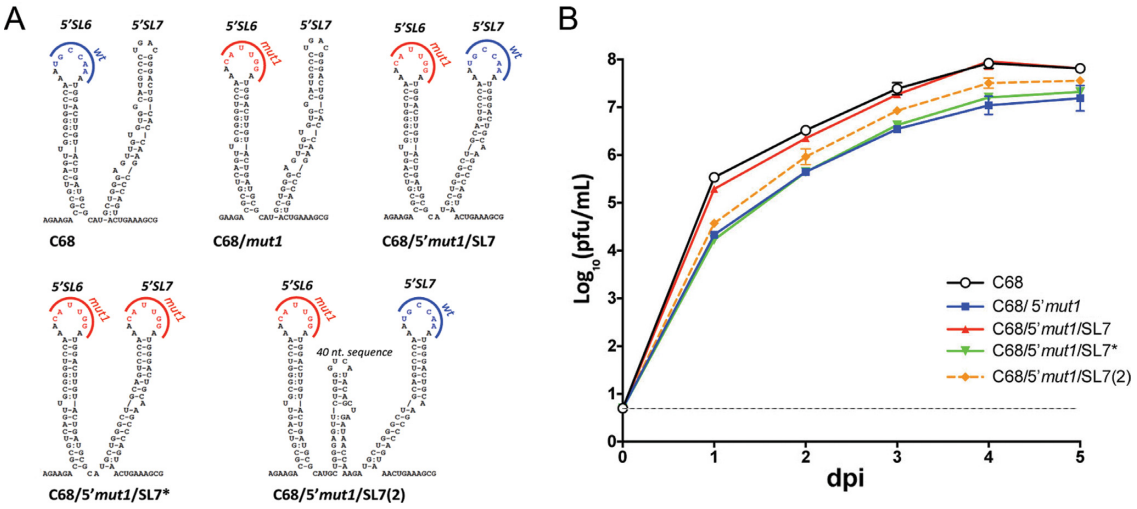

Figure 9. Functional kissing-loop contact between 5′and 3′ ends of LGTV genome can occur if hexanucleotide motif from the tip of 5′SL6 is relocated to the neighboring stem loop structure. (**A**) Schematic representations of viral genomes with nt mutations or 40 nt insertion that were engineered in 5′SL6 and/or 5′SL7 sequences of C68 virus in order to relocate the position of 5′ kissing-loop sequence. (**B**) Growth kinetics of parental C68 and its mutant derivatives in transfected Vero cells.

RepC58/3′*mut2* nLuc expression to a level similar to that of RepC58/5′*mut2*. It should be noted that the nLuc activity measured in RepC58/3′*mut2*-transfected cells was significantly reduced during the observation period probably due to deficiency in replicon amplification and its degradation by cellular ribonucleases.

To determine why mutations in 3′SL3 have a much stronger effect on nLuc expression compared to mutations in 5′SL6, we deleted almost the entire region of the polyprotein (2001 AAs from 880 to 2881) that comprised the non-structural proteins (from NS1 to NS5) of RepC58 or its derivatives (RepC58/5′*mut2*, RepC58/3′*mut2* and RepC58/5′3′*mut2*) carrying *mut2* substitutions (Figure 7A). Deletion of non-structural proteins allows direct comparison of the translation efficiency of resulting replicons (Rep*) and is not affected by interactions of the replicative complex with translated RNA. The kinetics of nLuc expression of Rep*C58 and Rep*C58/5′*mut2* were nearly identical, indicating that mutations in 5′SL6 only affect LGTV RNA genome replication but not ORF translation (Figure 7B and C). In contrast, insertion of *mut2* mutations in 3′SL3 of Rep*C58/3′*mut2* or Rep* C58/5′3′*mut2* reduced nLuc expression >3-fold compared to that of Rep*C58 identified as early as 2 h post-transfection, reaching 5.8-fold by 26 h (Figure 7C). These studies demonstrated that sequences located at the tip of 3′SL3 play functionally important roles in at least two distinct processes: (i) interaction with the 5′-end of LGTV genome via kissing-loop contact with 5′SL6 and (ii) regulation of viral RNA translation and/or stability. It appears that *mut2* substitutions in RepC58/5′3′*mut2* only restore kissing-loop interaction of 3′SL3 by increasing genomic RNA amplification (Figure 7B), but not the function(s) that control Rep*C58/5′3′*mut2* replicon RNA translation or stability (Figure 7C).

Dysfunctional kissing-loop contact can be compensated by a mutation that stabilizes a single pair of cyclization elements in LGTV genome. To better understand the mechanistic role of kissing-loop contact in virus replication, we sought to determine whether second-site mutation(s) may exist that compensate for disturbance or interference of kissing-loop interaction between 5′SL6 and 3′SL3. For that, C68/5′*mut2* and C68/3′*mut2* viruses were subjected to 10 serial passages in Vero cells, followed by sequence analysis of 5′- and 3′-genome termini. Interestingly, both viruses independently acquired the same U→C mutation at the base of 3′SL1 (Figure 8A), in the region that constitutes the 3′ strand of LGTV cyclization element (CYC). This mutation increases complementarity between 5′ cyclization sequence (5′CS) and 3′CS from 11 to 13 nt, which results in an m-fold predicted decrease in Gibbs free energy from −23.3 to −25.7 kcal (Figure 8B). To confirm that a U→C mutation in the 3′CS can compensate for the disruption of kissing-loop contact, we introduced this substitution (designated CS) into C68, C68/5′*mut2*, C68/3′*mut2* and C68/5′3′*mut2* viruses. This substitution increased growth of only C68/5′*mut2*/CS and C68/3′*mut2*/CS viruses with disrupted kissing-loop contact, but not of C68/CS and C68/5′3′*mut2*/CS (Figure 8C and D). These findings are in agreement with the hypothesis that the function of kissing-loops is to bring 5′ and 3′ ends of the LGTV genome together to initiate viral replication.

The 5′ kissing-loop can convey its function when relocated from its original position in the C gene. To address whether the primary location of 5′SL6 (and conserved hexanucleotide at its tip) in the LGTV genome is critical for formation of 5′-3′ kissing-loop contact, we relocated that structure from its natural position within the LGTV genome. For that, 5′SL7, which can be deleted without substantial effect on virus replication (Figure 3; C43 and C48 viruses), was modified in C68/5′*mut1* virus to attain a 5′SL6-like structure with the authentic UGCCAA hexanucleotide (wt) at its tip (Figure 9A). The resulting C68/5′*mut1*/SL7 virus reached a titer similar to unmodified C68 virus and was 10-fold higher compared to the parental C68/5′*mut1* virus (Figure 9B).

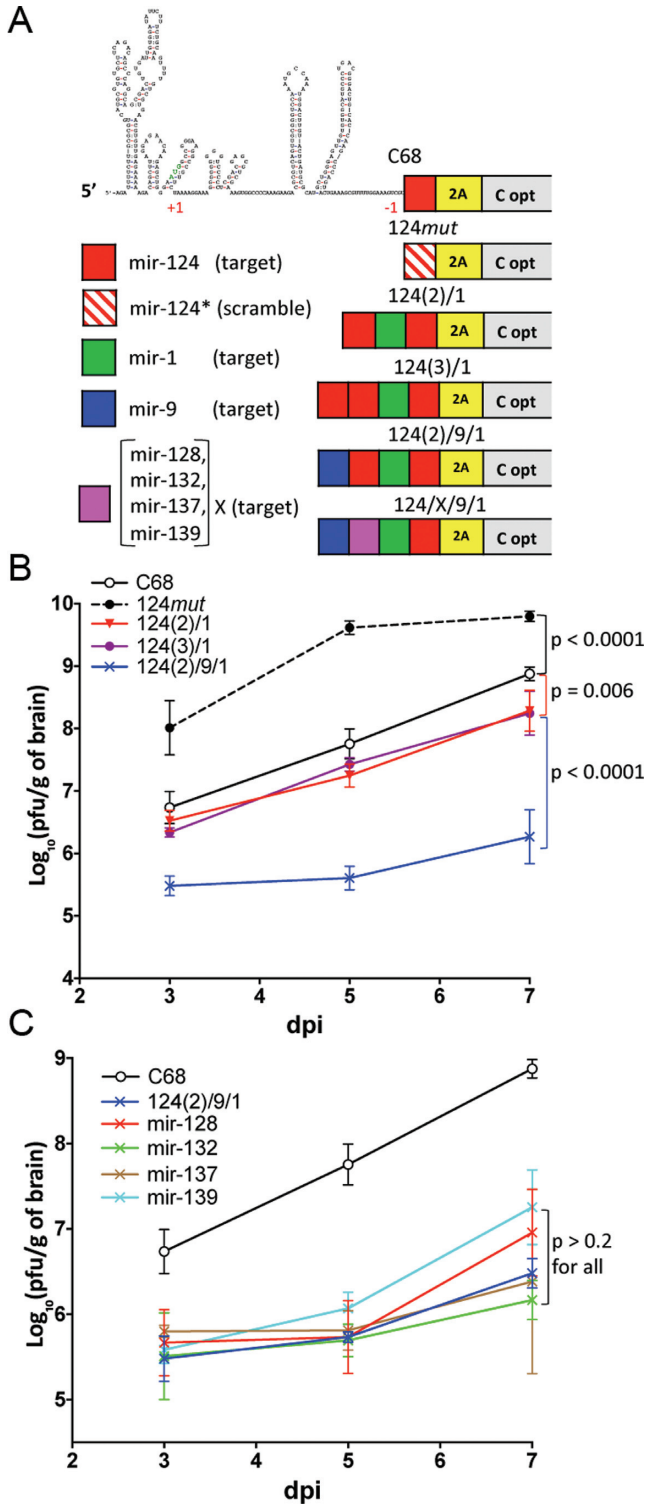

Figure 10. Effect of brain-specific miRNA target insertions into the DCGR on growth of LGTV in CNS of newborn mice. (**A**) Schematic representation of viruses with a single copy of mir-124 target or its scrambled sequence as well as with miRNA targets for mir-1, mir-9, mir-128, mir-132, mir-137 and mir-139. (**B** and **C**). Growth kinetics of miRNA-targeted viruses in mouse brains. Three-day-old mice were inoculated IC with 100 pfu of indicated virus, and brains from three mice in each group were collected at the indicated time points. Mean titers (±SD) of brain homogenates are shown. Differences in growth kinetics were compared using 2-way ANOVA. *P*-values were adjusted using Tukey's multiple comparison test.

To confirm that the increased growth of C68/5′*mut1*/SL7 virus was due to restored kissing-loop contact, the UGCCAA hexanucleotide sequence in the 5′SL7 of C68/5′*mut1*/SL7 was replaced with *mut1* sequence (Figure 9A). As expected, this resulted in a 10-fold lower titer of mutant virus in Vero cells compared to C68/5′*mut1*/SL7 (Figure 9B). These findings demonstrate that primary (original) location of the 5′ kissing-loop in the 5′SL6 of the virus genome is not absolute; it can be relocated to the 5′SL7 to accommodate functional interaction with the 3′ end of the virus genome. An additional attempt to further relocate the kissing-loop by introducing a 40 nt sequence between 5′SL6 and 5′SL7 had an attenuating effect on virus replication (Figure 9B; C68/5′*mut1*/SL7(2) virus). This suggests that there is a limit on how far the 5′ kissing-loop can be moved from the original position in the LGTV genome without affecting its functionality.

Application of LGTV with DCGR for vaccine development

Insertion of CNS-specific miRNA target sequences between DCGRs results in tissue-specific attenuation of LGTV. To determine if placement of miRNA target sequences between DCGRs interferes with the ability of miRNA machinery to inhibit LGTV replication in the central nervous system (CNS), we introduced a perfectly complementary mir-124 target sequence immediately after C68 AA sequence in the C68 genome (Figure 10A). Also, a scrambled mutant (control) virus (124*mut*) was generated, in which mir-124 target sequence was modified by synonymous substitutions in each of its seven encoding AA codons (Supplementary Figure S3). Such modification in the scrambled miRNA target prevents the miRNA-target recognition and binding by a cellular *RNA-induced silencing complex* (RISC) preloaded with mir-124 miRNA. When C68 and 124*mut* were evaluated in 3-day-old Swiss Webster mice infected IC with 100 pfu (corresponding to 10^4 lethal dose 50% for TP-21 virus), the 124mut virus grew significantly faster in the brains as compared to parental C68 virus (Figure 10B, $P < 0.0001$, 2-way ANOVA). To explore if placement of multiple miRNA target sequences in the DCGR can provide higher level of virus attenuation in the CNS, we modified C68 by introducing an additional target sequence for mir-124. In addition, a sequence for tick-specific mir-1, which is not expressed in Vero cells or mouse brain (8), was placed between two mir-124 targets to generate 124(2)/1 virus. No adverse effect was detected on replication of 124(2)/1 virus in Vero cells as compared to C68 (Supplementary Figure S4). Interestingly, only a minor decrease in virus titers was detected in the brains of suckling mice infected with 124(2)/1 as compared to C68 virus, indicating that an increase in the copy number of mir-124 does not substantially improve virus attenuation (Figure 10B, $P < 0.006$; 2-way ANOVA). [Results of LGTV targeting for tick-specific miRNAs on viral growth in vertebrate and invertebrate hosts will be published elsewhere].

To determine if a combination of targets for heterotypic brain-specific miRNAs placed into the DCGR provides a stronger effect on LGTV attenuation in the CNS compared to monotype-specific miRNA targeting, we introduced target sequence for an additional brain-expressed mir-9 in front of the first copy of the mir-124 target sequence in

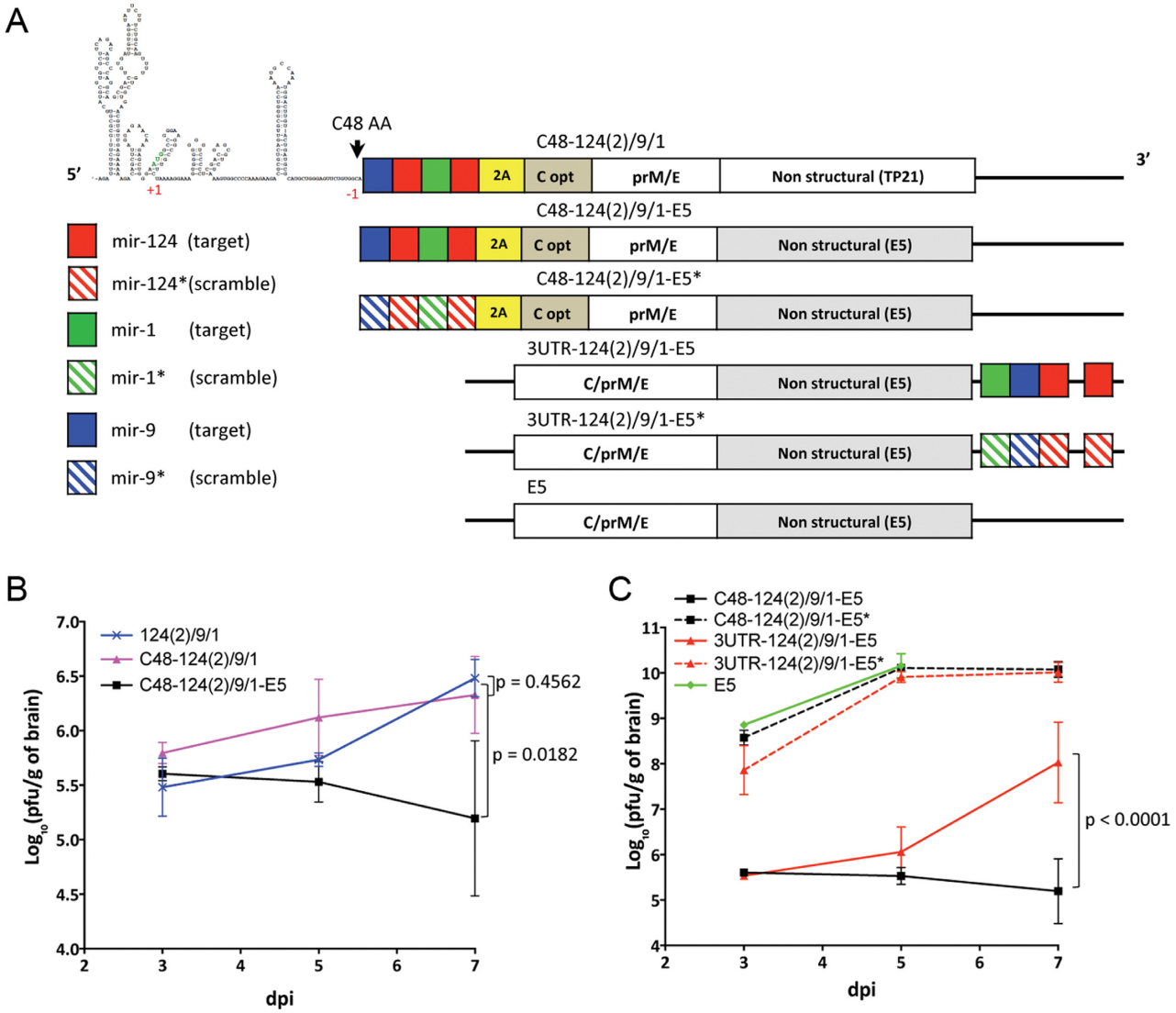

Figure 11. Insertion of miRNA target sequences for brain-specific miRNA into the DCGR resulted in more efficient LGTV attenuation in the CNS of newborn mice as compared with target insertion into 3′NCR. (**A**) Schematic representation of viruses used in this study. Genome sequence encoding the nonstructural proteins in the LGTV TP-21 strain and C48 virus was replaced with the corresponding sequence (gray area) derived from infectious cDNA clone of LGTV E5 strain (35). Target sequences for mir-1, mir-9 and mir-124 miRNAs or modified (scramble) miRNA targets were introduced in DCGR or 3′NCR as indicated. In the 3′NCR, a set of mir-1, mir-9 and mir-124 targets and a second copy of mir-124 target were inserted after nt 10 and 245, respectively. (**B** and **C**) Growth kinetics of miRNA-targeted viruses in mouse brains. Three-day-old mice were inoculated IC with a 100 pfu of each indicated virus. Mean titers (±SD) of three brain homogenates are shown for each time point. Differences in growth kinetics were compared between 124(2)/9/1 and miRNA targeted viruses (**B**), or between C48–124(2)/9/1-E5 and 3UTR-124(2)/9/1-E5 (**C**) using 2-way ANOVA. P-values were adjusted using Tukey's multiple comparison test.

the modified 124(2)/9/1 virus (Figure 10A). For comparison, the third mir-124 target sequence was introduced at the same position of 124(2)/1 to generate 124(3)/1 (Figure 10A). As expected, an increase in mir-124 targets copy number from 2 to 3 sequences had no effect on virus replication in the CNS (Figure 10B, $P = 0.9999$; 2-way ANOVA). In contrast, introduction of a mir-9 target into 124(2)/1 resulted in a significant [1.5 $\log_{10}$(pfu/g of brain)] decrease in virus titers in the brains of suckling mice (Figure 10B, $P < 0.0001$; 2-way ANOVA), but did not affect virus replication in Vero cells (Supplementary Figure S5), further supporting the role of miRNA-mediated regulation in controlling viral infection. Inclusion of target sequences for miRNAs, which are highly expressed in the CNS of newborn or adult mice (28,33), significantly restricted LGTV replication in the mouse brain but allowed the virus to efficiently replicate in simian Vero cells, in which the corresponding brain-specific miRNAs were not detected (7).

To explore if CNS-specific attenuation can be improved by an increase in the number of target sequences for heterotypic miRNAs, the first mir-124 target in 124(2)/9/1 virus was substituted with a single target for other miRNAs expressed in the CNS: mir-128, mir-132, mir-137 or mir-139 (Figure 10A) (7,28,34). Growth kinetics of viruses carrying these targets were similar to that of 124(2)/9/1 in Vero cells (Supplementary Figure S6) and in brains of suckling mice

(Figure 10C, $P > 0.2$ for 124(2)/9/1 and all other viruses; 2-way ANOVA), indicating that 124(2)/9/1 virus may have already reached the highest attenuation level that can be accomplished by the miRNA-mediated suppression.

The initial assessment of miRNA-mediated attenuation of viruses with DCGR in the CNS of mice was performed using LGTV containing C68 AA and/or C58 AA promoter regions (Supplementary Figure S3). As was demonstrated above, these promoters contain sequences dispensable for LGTV replication and can be substituted with the minimal C48 AA promoter without negative effect on virus fitness in cell culture (Figure 3C). As expected, replication of a newly engineered C48–124(2)/9/1 virus that contained a cassette of miRNA targets after the C48 AA promoter (Figure 11A) was indistinguishable compared to 124(2)/9/1 virus carrying target sequences downstream of the C58 AA promoter (Figure 11B, $P = 0.4562$; 2-way ANOVA). This indicates that miRNA-mediated attenuation of LGTV replication in the CNS is not affected by proximity of *cis*-acting elements of the C48 AA promoter region with miRNA targets. Mutations or deletions were not detected in the inserted target region of C48-124(2)/9/1 after 10 consecutive passages in Vero cells.

Since the more attenuated strain of LGTV (designated E5) is used in our laboratory as a genetic background for development of TBEV vaccine candidates (35), we modified C48–124(2)/9/1 to generate C48–124(2)/9/1-E5 virus. This virus differs by five E5-specific AA substitutions ($N_{24}\rightarrow S$, $F_{250}\rightarrow Y$, and $F_{319}\rightarrow L$ in NS3; $T_{422}\rightarrow S$ and $R_{544}\rightarrow K$ in NS5) located in the non-structural NS3 and NS5 proteins. C48–124(2)/9/1 replicated slightly slower than C48–124(2)/9/1-E5 in Vero cells, but both reached a titer of 7.5 $\log_{10}$(pfu/ml) on day 5 post-transfection (Supplementary Figure S7). In contrast, growth of C48–124(2)/9/1-E5 was significantly inhibited in the brain of newborn mice infected IC (Figure 11B, $P = 0.0182$; 2-way ANOVA), indicating that an improved attenuation of miRNA targeted viruses in the CNS was provided by E5-specific AA substitutions.

Insertion of CNS-specific miRNA target sequences into DCGRs results in superior LGTV attenuation in mouse brain as compared to target placements into the 3′NCR. To compare the effects on virus fitness in the CNS by the placement of miRNA targets into the DCGR with that of other genome locations, we developed a 3UTR-124(2)/9/1-E5 virus, in which the same combination of miRNA targets as in C48–124(2)/9/1-E5 was introduced in the 3′ NCR (Figure 11A), a site that is more often used for miRNA-mediated regulation of gene expression (7,28,36). Overall, miRNA-targeting in the 3′NCR has a minimal effect on viral fitness in Vero cells, since growth kinetics of C48–124(2)/9/1-E5 and 3UTR-124(2)/9/1-E5 viruses were almost identical (Supplementary Figure S8). However, 3UTR-124(2)/9/1-E5 replicated more efficiently in the brains of suckling mice compared to C48–124(2)/9/1-E5 virus (Figure 11C, $P < 0.0001$, 2-way ANOVA). In contrast, growth of both control viruses (C48–124(2)/9/1-E5* and 3UTR-124(2)/9/1-E5* with scrambled miRNA targets) in the CNS was nearly identical (Figure 11C, $P = 0.3648$, 2-way ANOVA). Moreover, a delay in the onset of encephalitis and an improved survival in mice infected IC with C48–124(2)/9/1-E5 at a dose of 1 or 100 pfu was observed relative to mice infected with 3UTR-124(2)/9/1-E5 (Supplementary Figure S9). Taken together, these data indicate that placement of miRNA targets in the DCGR results in a $>10^5$-fold reduction in virus titer in the brain and has superior attenuating effect compared to targeting in the 3′NCR. Interestingly, sequence analysis of brain-derived viruses from mice that succumbed to C48–124(2)/9/1-E5 infection revealed that all emerged escape viruses had mutations and/or deletions of miRNA targets located downstream of the C43 AA promoter. Importantly, deletions never extended upstream into the 5′SL6 (Supplementary Figure S10) signifying the functionally important role of kissing-loops in the regulation of virus replication in cell culture and *in vivo*.

Insertion of CNS-specific miRNA target sequences into DCGRs does not interfere with development of protective immunity in mice. We examined whether the insertion of miRNA targets in the DCGR interferes with the development of adaptive immunity in mice. For that, 3-week-old C3H mice were infected intraperitoneally with 10^5 pfu of C48–124(2)/9/1-E5 virus or with diluent alone (mock). At 29 dpi, the mice were challenged with 10^4 pfu of wt LGTV strain (Table 1). Mice immunized with C48–124(2)/9/1-E5 developed high a level of neutralizing antibodies against TP-21 by 28 dpi, and no viremia was detected after challenge with wt LGTV strain [limit of detection 1.7 $\log_{10}$(pfu/ml)]. In contrast, challenge virus was detected in all mock-infected animals, with mean viremia of 2.7 $\log_{10}$(pfu/ml). Collectively, these data confirm that miRNA targeting in the DCGR does not interfere with development of protective humoral immunity in immunized animals (Table 1).

DISCUSSION

In this study, recombinant LGT viruses capable of stable expression of miRNA target sequences in the DCGR were developed that demonstrated superior attenuating characteristics in the CNS of mice compared to previously described miRNA-targeting strategies (Figure 11). This was achieved by separation of promoter/regulatory and structural functions of the C gene followed by stabilization of resulting sequences with combination of codon optimizing and ORF shifting mutations, thus preventing formation of wt-like genomes (Figure 2). Presence of multiple *cis*-acting elements within C48 AA promoter region was a critical factor contributing to increased genetic stability of viruses with miRNA targets in DCGR.

Cis-acting elements within C48 AA promoter region

Previous analysis of *cis*-acting elements located in C gene region of tick-borne flaviviruses primarily focused on TBEV and generated somewhat inconsistent results. Using an 'empty' TBEV replicon system (not expressing heterologous genes), it was previously demonstrated that as little as C7 AA region is required for the efficient TBEV genome replication in BHK-21 cells (17), and complete deletion of the C gene resulted in attenuation, but not in complete abolishment of replicon amplification. However, in subsequent

Table 1. Immunogenicity and protective efficacy of C48–124(2)/9/1-E5 virus in 3-week old C3H mice

Virus	No. of mice immunized	Viremia at 1 dpi log_{10}(pfu/ml)	$PRNT_{50}$ against TP-21 at 28 dpi	Viremia at 1 dpi after challenge with 10^4 pfu of LGTV; log_{10}(pfu/ml)
C48-124(2)/9/1-E5	5	3.15 ± 0.19	167 ± 98	<1.7
mock	5			2.74 ± 0.4

studies using firefly luciferase (fLuc) expressing TBEV replicons, it was shown that as many as C17 AA are required for wt-like level of RNA replication (18), and that mutations in 5′SL4, which spans up to position C15 AA, significantly reduce level of TBEV genome amplification (29). In the present study, even preservation of the C19 AA region was not sufficient for recovery of infectious LGTV (Figure 2D). This suggests that despite a close phylogenetic relation, a significant difference in composition of *cis*-acting elements within the C gene region might exist between LGTV and TBEV. Alternatively, observed discrepancies may result from a difference in cell lines used in these studies (Vero versus BHK-21). Interestingly, replication was not detected for TBEV replicons containing the C17 AA promoter region where sequence for fLuc was substituted with *Renilla* luciferase (rLuc) gene. However, replication of TBEV containing rLuc gene was restored if the C27 AA region was preserved (18). This suggests that additional *cis*-acting elements might be present downstream of the C17 AA region, which are involved in modulation of TBEV replication in a manner similar to that observed in LGTV, and the presence of fLuc sequence artificially mimics their effect.

In agreement with this hypothesis is the observation that mutations disrupting topology of 5′SL6, including the C24–42 AA region, significantly attenuated TBEV replication in porcine embryo kidney (PS) cells (19). Surprisingly, the same study documented only limited effect of the mutations at the tip of 5′SL6 on TBEV replication, which contradicts the results shown here, demonstrating that mutations in conserved hexanucleotide motif of the 5′SL6 tip have comparable effect on LGTV replication with mutations disrupting its stem-loop structure (Figures 5–7). These discrepancies, however, could be explained by differences in experimental approaches used in these two studies. The reliance on a full-length virus with a single copy of the authentic C gene apparently precluded Tuplin *et al*. (19) from generating and testing viruses bearing multiple mutations at the tip of 5′SL6 without affecting amino acid sequence of the C protein. Therefore, it is likely that only a partial effect of the hexanucleotide motif at the tip of 5′SL6 on virus replication could have been detected. As a final point, the regulatory role of C15-C24 AA region in tick-borne flavivirus replication has not been previously described in detail, and this study demonstrates that it can serve as a novel replication enhancer (Figure 4).

The 5′SL6 structure was determined to be the most 3′ distant *cis*-acting element within the C48 AA promoter region. It is located in the closest proximity to the site for miRNA target insertion into the DCGR and, thus, it has the highest potential to become genetically unstable due to miRNA mediated selective pressure (Supplementary Figure S10). Therefore, the functional role of 5′SL6 in virus replication was further analyzed. We found that:

(i) The 5′SL6 functions as a structural scaffold for the conserved hexanucleotide motif located at its tip. Mutations that destabilized the stem structure negatively affected the 5′SL6 functionality, but it could be regained by compensatory mutations that restored stem organization (Figure 5). Mutations introduced in the conserved hexanucleotide motif at the tip of 5′SL6 had the same effect on virus replication as mutations that disturbed stem structure organization (Figure 6).

(ii) The conserved hexanucleotide motif at the tip of 5′SL6 is engaged in complementary interaction with the hexanucleotide sequence located at the tip of m-fold predicted 3′SL3 (kissing-loop interaction). Compensatory mutations that restore sequence complementarity between sequences at the tips of 5′SL6 and 3′SL3 have a positive effect on virus growth in Vero cells (Figure 6).

(iii) Our replicon study showed that destabilization of kissing-loop contact results in attenuation of LGTV genome replication, but has no effect on RNA translation/stability (Figure 7).

(iv) Independent (convergent) selection of the same resuscitating U→C mutation in the 3′SL1 (Figure 8) of two viruses containing dysfunctional kissing-loop contacts, which resulted from substitutions in the 5′ or 3′ kissing-loop, further supports a conclusion that 5′SL6 and 3′SL3 are engaged in functional interactions. More importantly, this resuscitating mutation appeared at the 3′CS of CYC element and increases the region of complementarity between 5′CS and 3′CS from 11 to 13 nt. (Figure 8). Since the mutation that compensates for the missing 5′-3′ kissing-loop contact acts by increasing stability of long range CYC contact between 5′ and 3′ ends of LGTV genome, it can be suggested that the primary function of kissing-loops is to assist the CYC in bringing 5′ and 3′ ends of LGTV genome together to form a panhandle-like structure, which is necessary for efficient replication of virus genome (37). An additional mutation C→U, which was only selected in the 3′SL3 of C68/3′*mut2* after repeated passage of the virus in Vero cells, likely compensates for the loss of additional functions of 3′SL3 associated with 3′*mut2* substitution, such as regulation of RNA translation or RNA stability (Figure 7C). Similarly, mutations in 3′SL3 can potentially affect production of LGTV sfRNA, which was recently shown to be important regulator of flavivirus life cycle (38–40).

(v) The native position of 5′SL6 within the LGTV genome is not absolutely critical for the 5′-3′ kissing-loop interaction that regulate virus replication, and some de-

gree of position variability can be tolerated (Figure 9). This finding is consistent with the proposed role of 5′-3′ kissing-loop contact in facilitating viral genome cyclization. Similarly, an earlier study demonstrated that 5′ CS can also be relocated from its primary position without affecting TBEV replication (17), suggesting that the 5′-3′ kissing-loops and 5′CS-3′ CS contacts might play a similar/connected role in LGTV replication.

(vi) Finally, since the topology of 5′SL6 and 3′SL3 remained evolutionarily conserved (19,30), and the sequences of hexanucleotide motifs at the tips of 5′ and 3′ loops are invariant among tick-borne flaviviruses, it is proposed that the interaction of the genomic ends via kissing-loop contact is a common mechanism to regulate genome replication for members of the TBEV group of flaviviruses.

The role of cyclization elements has been extensively analyzed for the mosquito-borne flaviviruses [reviewed in (41)], however, it received only limited attention for the TBEV group. In the case of mosquito-borne flaviviruses, it was previously shown that there are two pairs of inverted complementary sequences present at 5′ and 3′ genome ends that mediate genome cyclization (42–45). One pair of perfect complementarity consists of sequences located downstream of the initiation AUG codon (5′CS) and in the base of 3′SL1 (3′CS). The second pair of sequence complementarity (UAR) is formed by nts located upstream of the AUG codon (hence the name—*U*psteam *A*UG *R*egion), and the sequence that is a part of 3′SL1 (Figure 12). Some authors also recognize an additional pair of inverted complementary sequences designated as downstream AUG region located between UAR and 5′CS (46); however, its involvement in long distance RNA interaction remains uncertain. Functional studies have shown that complementarity between nucleotides within 5′ and 3′ CSs and UARs is critical for genomic RNA replication, but it does not affect RNA translation (37,43,45,47–50). Using atomic force microscopy Alvarez *et al.* were able to directly demonstrate DENV genome cyclization, which was affected by mutations in CYC and UAR sequences (37).

Interestingly, the m-fold RNA folding algorithm recognizes both pairs of inverted complementary sequences at the 5′ and 3′ ends of mosquito-borne flavivirus genomes (Figure 12). In contrast, the same program only recognizes a single pair of CYC sequences for most members of the TBEV serocomplex. This pair, designated as 5′CS-3′CS (Figure 12), occupies the same position as UAR pair in mosquito-borne viruses. The m-fold RNA analysis predicts that in linear form the 3′CS region of mosquito-borne viruses folds into a relatively unstable 3′SL2, which becomes a part of 5′CS-3′CS complex during genome cyclization. In contrast this region in tick-borne viruses typically folds into complex secondary structures involving thermodynamically stable 3′SL2 and 3′SL3, which is predicted not to interact with sequences located at the 5′ end of the genome (Figure 12). This is in agreement with the earlier suggestion that in contrast to mosquito-borne viruses, members of the tick-borne phylogroup possess only a single pair of functional cyclization elements (17). As proposed (41,43), a switch from the 'linear' to the cyclized form of flavivirus genome is required for the initiation of minus strand RNA synthesis of the genome. In this context, long-distance genome interaction via kissing-loop contact of tick-borne flaviviruses, described here, could be viewed as a functional homolog of a second pair of cyclization elements of mosquito-borne viruses, thus filling an apparent gap between these groups of flaviviruses in mechanisms of viral RNA replication.

It remains to be addressed why kissing-loop contacts were preserved during evolution of tick-bone flaviviruses despite the fact that their effect can be almost completely compensated by a single 3′CS mutation (Figure 8C and D). It is possible that kissing-loop contacts are more important for LGTV replication in tick vectors as opposed to the mammalian host. However, the growth kinetics of LGTV with and without compensating 3′CS mutation in tick-derived ISE6 cells mostly mirrored that of Vero cells (Supplementary Figure S11). Nevertheless, different results might have been obtained if live ticks (not a laboratory cell line) would have been tested. Alternatively, kissing-loop contacts might be indispensable for replications of tick-borne flaviviruses in immune-competent vertebrate organism.

Application of LGTV with the DCGR for vaccine studies

This study demonstrated that insertion of targets for brain-specific miRNA into the DCGR results in a selective attenuation of LGTV replication in the CNS (Figures 10 and 11). The developed strategy for placement of miRNA targets into the DCGR resulted in a lower LGTV titer in mouse brain and prolonged survival of infected newborn mice compared to miRNA-targeting in the 3′NCR (Figure 11, Supplementary Figure S9). The miRNA-mediated virus attenuation was cell/tissue-type specific, as growth of LGTV with miRNA targets in the DCGR was not inhibited in Vero cells or in the periphery of mice and it did not interfere with the development of protective immunity in immunized animals (Table 1). This demonstrates that the suggested strategy presents a suitable approach for development of a safe, live attenuated vaccine candidate against tick-borne flaviviruses and would reduce risks associated with a reversion of the vaccine virus to virulent phenotype.

The mechanism explaining increased safety of viruses with miRNA targets inserted into the DCGR as compared to LGTV with the same combination of targets in the 3′NCR is not completely clear. It was postulated that miRNA-mediated gene silencing is more efficient if targets are located in the 3′NCR due to a lack of interference between the RISC and translating ribosomes (51–54). This should favor suppression of viruses with miRNA targets inserted into the 3′NCR over the DCGR, which is a part of the viral ORF. However, previous studies showed that the 3′NCR is the least conserved part of a flavivirus genome, which can tolerate significant rearrangements, alterations and deletions (35,55,56). Therefore, the probability of deletion mutants expelling miRNA target sites under miRNA-mediated selective pressure to generate a replication-competent virus would be considerably higher for viruses targeted in the 3′NCR than in the DCGR, because miRNA targets in the DCGR are tightly constrained by two functional regions (*cis*-acting elements within the

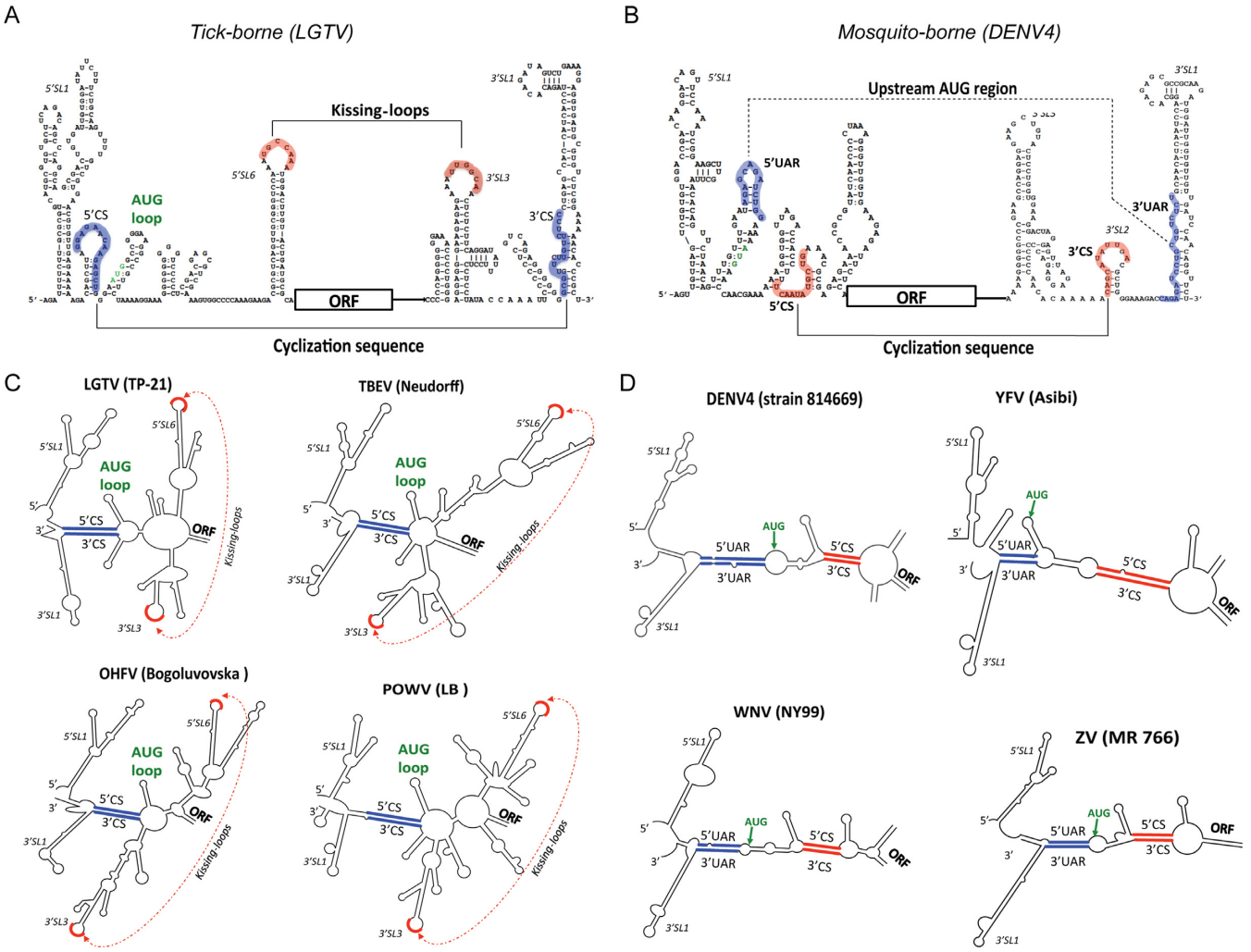

Figure 12. Structural comparison of tick-borne and mosquito-borne flavivirus genomic regions involved in viral RNA cyclization. (**A** and **B**) Stem-loop structures in 5′ and 3′ termini of LGTV (**A**) and dengue type 4 virus (**B**) genomes are shown in a linear configuration. Regions potentially involved in putative interactions between 5′ and 3′ termini of RNA genome are highlighted as blue and red sequences. (**C** and **D**) Predicted structures of genomic RNAs are given in the circular configurations for representative members of tick-borne (**C**) and mosquito-borne (**D**) flaviviruses. Secondary RNA structures were predicted using m-fold web server for nucleic acid folding as described in materials and methods. Note: 5′UAR is the 5′upstream AUG codon region, which is complementary to the 3′end region of the virus genome (3′UAR).

C48 AA promoter and the 2A protease of FMDV that is responsible for N-terminal cleavage of full-length C-protein). Moreover, placement of miRNA targets into an ORF-shifted region of the truncated C-protein gene imposes an additional restriction on configuration of virus escape mutants, since only restoration of correct ORF translation can be tolerated. In agreement with this assumption is the observation that only short deletions located between 5′SL6 and the 2A protease gene were observed (Supplementary Figure S10), whereas analysis of viruses with targets in the 3′NCR revealed an array of deletions of various sizes occurring in different locations (9,28). In agreement with the probability hypothesis is the fact that two out of six (33%) escape C48–124(2)/9/1-E5 mutants did not acquire large deletions eradicating miRNA targets. Instead, several nt substitutions occurred simultaneously in each of CNS-specific miRNA targets inserted in the DCGR (Supplementary Figure S10). This trend of virus escape has never been observed for viruses with multiple targets in the 3′NCR, and only mutants with deletions of all miRNA targets and genome sequences located between them were recovered from brains of moribund mice (9,28).

Increasing the number of target copies (2 or 3 copies) for brain-specific mir-124 in the DCGR displayed almost no effect on LGTV replication in the CNS compared to growth of virus with a single mir-124 target copy. In contrast, combination of targets for two distinct brain-enriched miRNAs (mir-9 and mir-124) in the DCGR resulted in a significant decrease in LGTV titers in the CNS of mice (Figure 10). This likely reflects differential expression and distribution of these miRNAs within the CNS. Mir-124 is exclusively expressed in cells of a neuronal origin (57,58), while mir-9 is also expressed in microglial cells, which are derived from myeloid precursor cells (59,60). This may result in additional restriction in replication of mir-124 and mir-9 targeted viruses in the brain tissues. Alternatively, relative

distance between mir-124 targets in 124(2)/1 and 124(3)/1 viruses could have been selected in a way that does not favor cooperative RISC interaction with these targets (61). Therefore, introduction of a single copy of heterologous mir-9 target improved the LGTV attenuation because it could act independently from a mir-124 target (not being involved in cooperative RISC interactions with mir-124 target). This data (Figure 10) is in good agreement with that observed previously (28). The simultaneous tandem targeting of the chimeric TBEV/DEN4 flavivirus genome for two different brain-expressed miRNAs (mir-9 and mir-124) was more efficient in reducing virus neurovirulence in mice than the targeting of two or three tandem targets for mir-124 miRNA alone.

Further addition of miRNA targets for other brain-expressed miRNAs (mir-128, -132, -137 or -139) into the DCGR did not decrease LGTV titer in the mice brain (Figure 10). It can be hypothesized that cell-type specificity of miRNA expression as well as the distribution of these miRNAs within CNS likely overlapped with the expression pattern of mir-9 and/or mir-124. However, it has been shown that the miRNA targeting of a single region of the LGTV genome even with a combination of targets for the most expressed brain-specific miRNAs is not sufficient to attain an appropriate level of virus attenuation expected from a safe vaccine candidate (62,63). Within this study viruses were observed to escape from miRNA suppression and cause fatal encephalitis (Supplementary Figure S10). Therefore, simultaneous miRNA co-targeting of multiple genome regions will be required to achieve this safety goal, as was demonstrated previously for TBEV/DEN4 chimeric virus (9,28). Alternatively, miRNA targeting of the DCGR developed here might be implemented in combination with other attenuating strategies for restricting pathogenicity of tick-borne flaviviruses [(24) and reviewed in (64)].

Finally, 5′ *cis*-acting elements identified within the LGTV coding region should be useful for constructing viruses expressing heterologous genes of interest (not only miRNA targets) in the genetic background of infectious LGTV or other tick-borne flaviviruses. Understanding the role of the 5′-regulatory region in flavivirus replication should improve design of efficient replicon systems for basic studies and for development of novel single round vaccine candidates against TBEV and other tick-borne flaviviruses.

SUPPLEMENTARY DATA

Supplementary Data are available at NAR Online.

ACKNOWLEDGEMENT

We thank Dr Ulrike Munderloh (University of Minnesota) for providing ISE6 cells, as well as Evgeniya Volkova, Dr Charles McGee and Dr Stephen S. Whitehead for critically reviewing the manuscript.

FUNDING

Division of Intramural Research Program of the National Institute of Allergy and Infectious Diseases; National Institutes of Health. Funding for open access charge: Division of Intramural Research Program of the National Institute of Allergy and Infectious Diseases; National Institutes of Health.

Conflict of interest statement. None declared.

REFERENCES

1. Lasala,P.R. and Holbrook,M. (2010) Tick-borne flaviviruses. *Clin. Lab. Med.*, **30**, 221–235.
2. Gritsun,T.S., Lashkevich,V.A. and Gould,E.A. (2003) Tick-borne encephalitis. *Antiviral Res.*, **57**, 129–146.
3. Smith,C.E. (1956) A virus resembling Russian spring-summer encephalitis virus from an ixodid tick in Malaya. *Nature*, **178**, 581–582.
4. Pletnev,A.G. and Men,R. (1998) Attenuation of the Langat tick-borne flavivirus by chimerization with mosquito-borne flavivirus dengue type 4. *Proc. Natl. Acad. Sci. U.S.A.*, **95**, 1746–1751.
5. Price,W.H., Thind,I.S., Teasdall,R.D. and O'Leary,W. (1970) Vaccination of human volunteers against Russian spring-summer (RSS) virus complex with attenuated Langat E5 virus. *Bull. World Health Organ.*, **42**, 89–94.
6. Smorodincev,A.A. and Dubov,A.V. (1986) Live vaccines against tick-borne encephalitis. In: Smorodincev,AA (ed). *Tick-borne encephalitis and its vaccine prophylaxis*. Meditsina, Leningrad, pp. 190–211.
7. Heiss,B.L., Maximova,O.A. and Pletnev,A.G. (2011) Insertion of microRNA targets into the flavivirus genome alters its highly neurovirulent phenotype. *J. Virol.*, **85**, 1464–1472.
8. Tsetsarkin,K.A., Liu,G., Kenney,H., Bustos-Arriaga,J., Hanson,C.T., Whitehead,S.S. and Pletnev,A.G. (2015) Dual miRNA targeting restricts host range and attenuates neurovirulence of flaviviruses. *PLoS Pathog.*, **11**, e1004852.
9. Teterina,N.L., Liu,G., Maximova,O.A. and Pletnev,A.G. (2014) Silencing of neurotropic flavivirus replication in the central nervous system by combining multiple microRNA target insertions in two distinct viral genome regions. *Virology*, **456–457**, 247–258.
10. Shustov,A.V., Mason,P.W. and Frolov,I. (2007) Production of pseudoinfectious yellow fever virus with a two-component genome. *J. Virol.*, **81**, 11737–11748.
11. McGee,C.E., Shustov,A.V., Tsetsarkin,K., Frolov,I.V., Mason,P.W., Vanlandingham,D.L. and Higgs,S. (2010) Infection, dissemination, and transmission of a West Nile virus green fluorescent protein infectious clone by Culex pipiens quinquefasciatus mosquitoes. *Vector Borne Zoonotic Dis.*, **10**, 267–274.
12. Schoggins,J.W., Dorner,M., Feulner,M., Imanaka,N., Murphy,M.Y., Ploss,A. and Rice,C.M. (2012) Dengue reporter viruses reveal viral dynamics in interferon receptor-deficient mice and sensitivity to interferon effectors in vitro. *Proc. Natl. Acad. Sci. U.S.A.*, **109**, 14610–14615.
13. Groat-Carmona,A.M., Orozco,S., Friebe,P., Payne,A., Kramer,L. and Harris,E. (2012) A novel coding-region RNA element modulates infectious dengue virus particle production in both mammalian and mosquito cells and regulates viral replication in Aedes aegypti mosquitoes. *Virology*, **432**, 511–526.
14. de Borba,L., Villordo,S.M., Iglesias,N.G., Filomatori,C.V., Gebhard,L.G. and Gamarnik,A.V. (2015) Overlapping local and long-range RNA-RNA interactions modulate dengue virus genome cyclization and replication. *J. Virol.*, **89**, 3430–3437.
15. Liu,Z.Y., Li,X.F., Jiang,T., Deng,Y.Q., Zhao,H., Wang,H.J., Ye,Q., Zhu,S.Y., Qiu,Y., Zhou,X. *et al.* (2013) Novel cis-acting element within the capsid-coding region enhances flavivirus viral-RNA replication by regulating genome cyclization. *J. Virol.*, **87**, 6804–6818.
16. Gebhard,L.G., Filomatori,C.V. and Gamarnik,A.V. (2011) Functional RNA elements in the dengue virus genome. *Viruses*, **3**, 1739–1756.
17. Kofler,R.M., Hoenninger,V.M., Thurner,C. and Mandl,C.W. (2006) Functional analysis of the tick-borne encephalitis virus cyclization elements indicates major differences between mosquito-borne and tick-borne flaviviruses. *J. Virol.*, **80**, 4099–4113.
18. Hoenninger,V.M., Rouha,H., Orlinger,K.K., Miorin,L., Marcello,A., Kofler,R.M. and Mandl,C.W. (2008) Analysis of the effects of alterations in the tick-borne encephalitis virus 3'-noncoding region

on translation and RNA replication using reporter replicons. *Virology*, **377**, 419–430.
19. Tuplin,A., Evans,D.J., Buckley,A., Jones,I.M., Gould,E.A. and Gritsun,T.S. (2011) Replication enhancer elements within the open reading frame of tick-borne encephalitis virus and their evolution within the Flavivirus genus. *Nucleic Acids Res.*, **39**, 7034–7048.
20. Campbell,M.S. and Pletnev,A.G. (2000) Infectious cDNA clones of Langat tick-borne flavivirus that differ from their parent in peripheral neurovirulence. *Virology*, **269**, 225–237.
21. Yamshchikov,V., Mishin,V. and Cominelli,F. (2001) A new strategy in design of +RNA virus infectious clones enabling their stable propagation in E. coli. *Virology*, **281**, 272–280.
22. Sambrook,J., Fritsch,E. and Maniatis,T. (1989) *Molecular Cloning: a Laboratory Manual*. 2nd edn. Cold Spring Harbor Laboratory, NY.
23. Bonaldo,M.C., Mello,S.M., Trindade,G.F., Rangel,A.A., Duarte,A.S., Oliveira,P.J., Freire,M.S., Kubelka,C.F. and Galler,R. (2007) Construction and characterization of recombinant flaviviruses bearing insertions between E and NS1 genes. *Virol. J.*, **4**, 1–16.
24. Engel,A.R., Rumyantsev,A.A., Maximova,O.A., Speicher,J.M., Heiss,B., Murphy,B.R. and Pletnev,A.G. (2010) The neurovirulence and neuroinvasiveness of chimeric tick-borne encephalitis/dengue virus can be attenuated by introducing defined mutations into the envelope and NS5 protein genes and the 3' non-coding region of the genome. *Virology*, **405**, 243–252.
25. Team,R.C. (2015) *R: A language and environment for statistical computing*, R Foundation for statistical computing, Vienna.
26. Pletnev,A.G., Bray,M., Hanley,K.A., Speicher,J. and Elkins,R. (2001) Tick-borne Langat/mosquito-borne dengue flavivirus chimera, a candidate live attenuated vaccine for protection against disease caused by members of the tick-borne encephalitis virus complex: evaluation in rhesus monkeys and in mosquitoes. *J. Virol.*, **75**, 8259–8267.
27. Zuker,M. (2003) Mfold web server for nucleic acid folding and hybridization prediction. *Nucleic Acids Res.*, **31**, 3406–3415.
28. Heiss,B.L., Maximova,O.A., Thach,D.C., Speicher,J.M. and Pletnev,A.G. (2012) MicroRNA targeting of neurotropic flavivirus: effective control of virus escape and reversion to neurovirulent phenotype. *J. Virol.*, **86**, 5647–5659.
29. Rouha,H., Hoenninger,V.M., Thurner,C. and Mandl,C.W. (2011) Mutational analysis of three predicted 5'-proximal stem-loop structures in the genome of tick-borne encephalitis virus indicates different roles in RNA replication and translation. *Virology*, **417**, 79–86.
30. Gritsun,D.J., Jones,I.M., Gould,E.A. and Gritsun,T.S. (2014) Molecular archaeology of Flaviviridae untranslated regions: duplicated RNA structures in the replication enhancer of flaviviruses and pestiviruses emerged via convergent evolution. *PLoS One*, **9**, e92056.
31. Elshuber,S., Allison,S.L., Heinz,F.X. and Mandl,C.W. (2003) Cleavage of protein prM is necessary for infection of BHK-21 cells by tick-borne encephalitis virus. *J. Gen. Virol.*, **84**, 183–191.
32. Pletnev,A.G., Bray,M. and Lai,C.J. (1993) Chimeric tick-borne encephalitis and dengue type 4 viruses: effects of mutations on neurovirulence in mice. *J. Virol.*, **67**, 4956–4963.
33. Bak,M., Silahtaroglu,A., Moller,M., Christensen,M., Rath,M.F., Skryabin,B., Tommerup,N. and Kauppinen,S. (2008) MicroRNA expression in the adult mouse central nervous system. *RNA*, **14**, 432–444.
34. Sempere,L.F., Freemantle,S., Pitha-Rowe,I., Moss,E., Dmitrovsky,E. and Ambros,V. (2004) Expression profiling of mammalian microRNAs uncovers a subset of brain-expressed microRNAs with possible roles in murine and human neuronal differentiation. *Genome Biol.*, **5**, R13.
35. Pletnev,A.G. (2001) Infectious cDNA clone of attenuated Langat tick-borne flavivirus (strain E5) and a 3' deletion mutant constructed from it exhibit decreased neuroinvasiveness in immunodeficient mice. *Virology*, **282**, 288–300.
36. Pham,A.M., Langlois,R.A. and TenOever,B.R. (2012) Replication in cells of hematopoietic origin is necessary for Dengue virus dissemination. *PLoS pathogens*, **8**, e1002465.
37. Alvarez,D.E., Lodeiro,M.F., Luduena,S.J., Pietrasanta,L.I. and Gamarnik,A.V. (2005) Long-range RNA-RNA interactions circularize the dengue virus genome. *J. Virol.*, **79**, 6631–6643.
38. Pijlman,G.P., Funk,A., Kondratieva,N., Leung,J., Torres,S., van der Aa,L., Liu,W.J., Palmenberg,A.C., Shi,P.Y., Hall,R.A. *et al.* (2008) A highly structured, nuclease-resistant, noncoding RNA produced by flaviviruses is required for pathogenicity. *Cell Host Microbe*, **4**, 579–591.
39. Manokaran,G., Finol,E., Wang,C., Gunaratne,J., Bahl,J., Ong,E.Z., Tan,H.C., Sessions,O.M., Ward,A.M., Gubler,D.J. *et al.* (2015) Dengue subgenomic RNA binds TRIM25 to inhibit interferon expression for epidemiological fitness. *Science*, **350**, 217–221.
40. Funk,A., Truong,K., Nagasaki,T., Torres,S., Floden,N., Balmori Melian,E., Edmonds,J., Dong,H., Shi,P.Y. and Khromykh,A.A. (2010) RNA structures required for production of subgenomic flavivirus RNA. *J. Virol.*, **84**, 11407–11417.
41. Brinton,M.A. and Basu,M. (2015) Functions of the 3' and 5' genome RNA regions of members of the genus Flavivirus. *Virus Res.*, **206**, 108–119.
42. Hahn,C.S., Hahn,Y.S., Rice,C.M., Lee,E., Dalgarno,L., Strauss,E.G. and Strauss,J.H. (1987) Conserved elements in the 3' untranslated region of flavivirus RNAs and potential cyclization sequences. *J. Mol. Biol.*, **198**, 33–41.
43. Khromykh,A.A., Meka,H., Guyatt,K.J. and Westaway,E.G. (2001) Essential role of cyclization sequences in flavivirus RNA replication. *J. Virol.*, **75**, 6719–6728.
44. Thurner,C., Witwer,C., Hofacker,I.L. and Stadler,P.F. (2004) Conserved RNA secondary structures in Flaviviridae genomes. *J. Gen. Virol.*, **85**, 1113–1124.
45. Zhang,B., Dong,H., Stein,D.A., Iversen,P.L. and Shi,P.Y. (2008) West Nile virus genome cyclization and RNA replication require two pairs of long-distance RNA interactions. *Virology*, **373**, 1–13.
46. Friebe,P. and Harris,E. (2010) Interplay of RNA elements in the dengue virus 5' and 3' ends required for viral RNA replication. *J. Virol.*, **84**, 6103–6118.
47. Alvarez,D.E., De Lella Ezcurra,A.L., Fucito,S. and Gamarnik,A.V. (2005) Role of RNA structures present at the 3'UTR of dengue virus on translation, RNA synthesis, and viral replication. *Virology*, **339**, 200–212.
48. Lo,M.K., Tilgner,M., Bernard,K.A. and Shi,P.Y. (2003) Functional analysis of mosquito-borne flavivirus conserved sequence elements within 3' untranslated region of West Nile virus by use of a reporting replicon that differentiates between viral translation and RNA replication. *J. Virol.*, **77**, 10004–10014.
49. Corver,J., Lenches,E., Smith,K., Robison,R.A., Sando,T., Strauss,E.G. and Strauss,J.H. (2003) Fine mapping of a cis-acting sequence element in yellow fever virus RNA that is required for RNA replication and cyclization. *J. Virol.*, **77**, 2265–2270.
50. Alvarez,D.E., Filomatori,C.V. and Gamarnik,A.V. (2008) Functional analysis of dengue virus cyclization sequences located at the 5' and 3'UTRs. *Virology*, **375**, 223–235.
51. Filipowicz,W., Bhattacharyya,S.N. and Sonenberg,N. (2008) Mechanisms of post-transcriptional regulation by microRNAs: are the answers in sight? *Nat. Rev. Genet.*, **9**, 102–114.
52. Bartel,D.P. (2009) MicroRNAs: target recognition and regulatory functions. *Cell*, **136**, 215–233.
53. Gu,S., Jin,L., Zhang,F., Sarnow,P. and Kay,M.A. (2009) Biological basis for restriction of microRNA targets to the 3' untranslated region in mammalian mRNAs. *Nat. Struct. Mol. Biol.*, **16**, 144–150.
54. Grimson,A., Farh,K.K., Johnston,W.K., Garrett-Engele,P., Lim,L.P. and Bartel,D.P. (2007) MicroRNA targeting specificity in mammals: determinants beyond seed pairing. *Mol. Cell*, **27**, 91–105.
55. Men,R., Bray,M., Clark,D., Chanock,R.M. and Lai,C.J. (1996) Dengue type 4 virus mutants containing deletions in the 3' noncoding region of the RNA genome: analysis of growth restriction in cell culture and altered viremia pattern and immunogenicity in rhesus monkeys. *J. Virol.*, **70**, 3930–3937.
56. Mandl,C.W., Holzmann,H., Meixner,T., Rauscher,S., Stadler,P.F., Allison,S.L. and Heinz,F.X. (1998) Spontaneous and engineered deletions in the 3' noncoding region of tick-borne encephalitis virus: construction of highly attenuated mutants of a flavivirus. *J. Virol.*, **72**, 2132–2140.
57. Smirnova,L., Grafe,A., Seiler,A., Schumacher,S., Nitsch,R. and Wulczyn,F.G. (2005) Regulation of miRNA expression during neural cell specification. *Eur. J. Neurosci.*, **21**, 1469–1477.

58. Makeyev,E.V., Zhang,J., Carrasco,M.A. and Maniatis,T. (2007) The MicroRNA miR-124 promotes neuronal differentiation by triggering brain-specific alternative pre-mRNA splicing. *Mol. Cell*, **27**, 435–448.
59. Yao,H., Ma,R., Yang,L., Hu,G., Chen,X., Duan,M., Kook,Y., Niu,F., Liao,K., Fu,M. *et al.* (2014) MiR-9 promotes microglial activation by targeting MCPIP1. *Nat. Commun.*, **5**, 4386.
60. Liu,G.D., Zhang,H., Wang,L., Han,Q., Zhou,S.F. and Liu,P. (2013) Molecular hydrogen regulates the expression of miR-9, miR-21 and miR-199 in LPS-activated retinal microglia cells. *Int. J. Ophthalmol.*, **6**, 280–285.
61. Saetrom,P. and Snove,O. Jr (2007) Robust machine learning algorithms predict microRNA genes and targets. *Methods Enzymol.*, **427**, 25–49.
62. Monath,T.P. (2005) Yellow fever vaccine. *Expert Rev. Vaccines*, **4**, 553–574.
63. Halstead,S.B. and Jacobson,J. (2008) Japanese encephalitis virus vaccines. In: Plotkin,S, Orenstein,W and Offit,P (eds). *Vaccines*. Elsevier, Philadelphia, pp. 311–352.
64. Kofler,R.M., Heinz,F.X. and Mandl,C.W. (2004) A novel principle of attenuation for the development of new generation live flavivirus vaccines. *Arch. Virol. Suppl.*, **18**, 191–200.